Hydrodynamic flow and concentration gradients in the gut enhance neutral bacterial diversity

Darka Labavić[1], Claude Loverdo[1,*] and Anne-Florence Bitbol[2,*]

[1]*Sorbonne Université, CNRS, Institut de Biologie Paris-Seine, Laboratoire Jean Perrin (UMR 8237), F-75005 Paris, France,*

[2]*Institute of Bioengineering, School of Life Sciences, École Polytechnique Fédérale de Lausanne (EPFL), CH-1015 Lausanne, Switzerland,*
*Equal contribution.

May 14, 2021

Abstract

The gut microbiota features important genetic diversity, and the specific spatial features of the gut may shape evolution within this environment. We investigate the fixation probability of neutral bacterial mutants within a minimal model of the gut that includes hydrodynamic flow and resulting gradients of food and bacterial concentrations. We find that this fixation probability is substantially increased compared to an equivalent well-mixed system, in the regime where the profiles of food and bacterial concentration are strongly spatially-dependent. Fixation probability then becomes independent of total population size. We show that our results can be rationalized by introducing an active population, which consists of those bacteria that are actively consuming food and dividing. The active population size yields an effective population size for neutral mutant fixation probability in the gut.

Introduction

In the human body, bacteria are approximately as numerous as human cells, and about 99% of these bacteria are located in the digestive tract [1]. The gut microbiota is very diverse, and collectively harbors more genes than there are human genes [2]. One source of this genetic diversity is evolution occurring within the gut, which is the natural environment of these bacteria. Such evolution can have important public health implications, as the gut can constitute a reservoir of antibiotic resistance, both in humans and in farm animals [3]. How does the environment in the gut affect the evolution of bacteria? A crucial feature of the gut is the flow of its contents along its main axis, and the associated gradients of concentration of food and bacteria. Going downstream along this axis, food is first ingested, then simple nutrients are absorbed by the body, next more complex molecules are broken down by bacteria, and eventually what remains of the food exits the system, together with many bacteria, which make up from a quarter to half of fecal mass [4]. These features yield a very particular spatial structure that can impact the evolution of bacteria.

Evolutionary models that investigate population spatial structure generally consider discrete patches of population with migrations between them, and the same environment in each of them [5–13]. Complex spatial structures are investigated through models on graphs where each individual [14–17] or each patch of population [18–21] occupies a node of the graph. Population structure can impact the rapidity of adaption [22–28] because local competition can allow the maintenance of larger genetic diversity. In simple population structures where migration is symmetric between patches [5, 6], the fixation probability of a mutant is unaffected by population structure [7, 8], unless extinctions of patches occur [11]. However, more complex population structures with asymmetric migrations can impact the fixation probabilities of beneficial and deleterious mutants [13, 14, 21]. In the case of the gut, the flow can be viewed as yielding asymmetric migrations, but the system is continuous. In large-scale turbulent systems, hydrodynamic flow has been shown to strongly impact fixation probabilities and fixation times [29–31]. In addition, environmental gradients, e.g. of antibiotic concentration, can strongly impact evolution [32–35]. How do population structure, hydrodynamic flow and gradients shape the evolution of bacteria in the gut microbiota?

Here, we propose a minimal model of evolution of bacteria in the gut. Because most bacteria in the human digestive tract are located in the bulk of the colon lumen [1, 36], we focus on this compartment. Since most bacteria in the digestive tract have no self-motility [37, 38], we consider that they are carried passively with the digesta. The motion of the digesta is complex, but it was shown in Refs. [39, 40] that it can be approximated as a one-dimensional flow with net velocity and effective diffusion representing mixing. Within this model of the gut that includes hydrodynamic flow and resulting gradients of food and bacterial concentrations, we ask how the fixation probability of a neutral mutant compares with that in an equivalent well-mixed chemostat. We find

1

that the structure of the gut can increase this fixation probability, specifically in the regime where the profiles of food and bacterial concentration are strongly spatially-dependent. In this regime, fixation probability becomes independent of total population size, in stark contrast with a well-mixed population, where fixation probability is inversely proportional to total population size [41, 42]. We show that this behavior can be understood by introducing the notion of active population, which corresponds to the fraction of the bacterial population that is actively consuming food and dividing.

Model and methods

Because the majority of bacteria in the human digestive tract are in the colon [36], we focus on this compartment. Within the colon, there are marked differences between bacteria associated to mucus and bacteria in the digesta, i.e. in the bulk of the colon lumen [36]. The latter constitute the majority of bacteria in the colon. Indeed, the surface area of the large intestine, including its folds, is about 2 square meters [43], while the mucus layer is about $100 - 300$ μm thick [44], and typically comprises a few 10^8 bacteria per milliliter in healthy samples [45], which leads to an order of magnitude of 10^{11} bacteria associated to mucus. This number is small compared to the total colon content, which is around 10^{14} bacteria [1]. Since mucus-associated bacteria constitute a small minority in the colon, and since their spatial structure and migration patterns are not well characterized, we focus on the bacteria present in the bulk of the colon lumen, and do not model the mucus layer. Henceforth, we refer to the colon lumen by "gut" for simplicity.

The dynamics of wild-type and mutant bacteria and food in the gut is described through three concentration fields, of food F, wild-type bacteria B and mutant bacteria M, based on the description of the coupled dynamics of food and bacteria (without mutants) developed in Ref. [39]. The gut is represented by a tube of length L and cross-section with surface area S (Figure 1A). In addition to this cylindrical symmetry, we neglect radial variations, and are left with a one dimensional model along the x axis, specifically a segment of length L. We assume a constant inflow of nutrients at the entrance of this gut segment and no inflow of bacteria. At the exit of the gut, we assume that there is a free outflow of both nutrients and bacteria. The dynamics is affected by the constant flow velocity v, by the mixing due to different mechanisms e.g. peristaltic movement, which is modelled by effective diffusion with diffusion coefficient D, and by the harvesting of the food by bacteria, which is described by a Hill-type function with Monod constant k, and is coupled to their growth which has maximal rate r. This leads to the following coupled partial differential equations:

$$\frac{\partial F}{\partial t} = D\frac{\partial^2 F}{\partial x^2} - v\frac{\partial F}{\partial x} - \frac{r}{\alpha}\frac{(B+M)F}{k+F}, \tag{1a}$$

$$\frac{\partial B}{\partial t} = D\frac{\partial^2 B}{\partial x^2} - v\frac{\partial B}{\partial x} + r\frac{BF}{k+F}, \tag{1b}$$

$$\frac{\partial M}{\partial t} = D\frac{\partial^2 M}{\partial x^2} - v\frac{\partial M}{\partial x} + r\frac{MF}{k+F}, \tag{1c}$$

with boundary conditions

$$-D\frac{\partial [F; B; M]}{\partial x}(x=0) + v[F; B; M](x=0) = [vF_{\text{in}}; 0; 0], \tag{2a}$$

$$-D\frac{\partial [F; B; M]}{\partial x}(x=L) = [0; 0; 0], \tag{2b}$$

where $[F; B; M]$ denotes a vector. Here vF_{in} is the food inflow at the entrance of the gut segment, while α denotes the yield of the conversion from food to bacteria. Note that there is zero inflow of bacteria, in agreement with observations that bacterial concentration in the smaller intestine is orders of magnitude smaller [36, 39, 40]. The boundary conditions at $x = L$ cancel the diffusive flux, corresponding to free outflow toward the downstream part of the colon.

In our study of the fate of mutants appearing in the gut, initial conditions are

$$F(t=0, x) = F^*(x), \tag{3a}$$

$$B(t=0, x) = B^*(x), \tag{3b}$$

$$M(t=0, x) = \begin{cases} M_0, |x - x_{\text{M}}| \leq \Delta x/2, \\ 0, |x - x_{\text{M}}| > \Delta x/2, \end{cases} \tag{3c}$$

where F^* and B^* represent the steady state of system 1 without mutant bacteria, while $x_{\text{M}} \in (0, L)$ is the position in the gut where the mutant appears, while Δx is a short length, taken equal to the spatial discrete

2

step in our numerical resolutions, and $M_0 \ll B(x_\mathrm{M})$ is the initial local concentration of mutant at this location. In practice, M_0 is set through $N_\mathrm{M} = M_0 S \Delta x$, where S is the surface area of the section of the gut, so that the total number N_M of mutants introduced in the system is always the same, and our results do not depend on Δx as long as it is small compared to the length scale over which concentrations vary.

The partial differential equations in Eqs. 1 with boundary conditions in Eqs. 2 and initial conditions in Eqs. 3 were solved numerically (Supplementary material Section S1, and code publicly available [46]).

Results

Spatial dependence of the steady-state bacterial concentration

Our aim is to study the fate of neutral mutants appearing in the gut, starting from initial conditions where the concentrations of food and wild-type bacteria are at steady state (see Eqs. 3). Therefore, we start by describing the steady-state profiles of food and wild-type bacteria in the mutant-free gut.

Steady-state solutions of the spatial model described by Eqs. 1 can strongly depend on the spatial coordinate x for some values of flow velocity v, and effective diffusion constant D, as exemplified by Figure 1B. Such strong spatial dependence is relevant in the ascending colon [40], which is our focus here. We quantify the spatial dependence of the concentration profiles through the difference between food concentration at the entrance and at the exit of the gut, normalized by the incoming food concentration F_in, namely $[F(0) - F(L)]/F_\mathrm{in}$. A heat map of this quantity is depicted in the $(v, D)-$parameter space in Figure 1C. We observe diverse levels of spatial dependence, ranging from strongly spatial profiles to quasi-flat ones, where the system is almost well-mixed and resembles a chemostat, or where bacteria are washed out by the flow [39, 40] (see Figure S1 for examples of concentration profiles across these regimes). There are two washout limits. First, for large diffusion coefficients, if the flow timescale is smaller than the replication timescale, bacteria exit the system before reproducing. Second, for small diffusion coefficients, on the timescale of one replication, if the characteristic length of flow is larger than that of diffusion, bacteria are washed out (see Supplementary material Section S3 and Figure S2).

To compare our spatial system to a well-mixed one, we consider a chemostat [47] with the same total number of bacterial reproductions N_R per unit time as in the spatial system, which is

$$N_\mathrm{R} = S \int_0^L B(x)\rho(x)dx, \tag{4}$$

where S is the surface area of the gut section, while $\rho(x)$ is the reproduction rate of bacteria, which can be expressed using food concentration as in Eqs. 1:

$$\rho(x) = r\frac{F(x)}{k + F(x)}. \tag{5}$$

This reproduction rate strongly depends on the spatial coordinate in the spatial regime of the concentration profiles, see Figure 1B. Once the total number of reproductions is matched, it is possible to impose an additional matching condition, and we consider three possibilities for it in the Supplementary material (see Section S4). These matching conditions allow to set the parameters characterizing the chemostat matching the spatial system, namely its dilution rate, food inflow and volume. In all cases, we observe that matching chemostats feature extreme values for some of these parameters (see Figure S3), which arises from the very small outflow of food in the spatial system (see Supplementary material Section S4). These results emphasize that the large intestine is a highly efficient system for converting unabsorbed nutrients into bacteria.
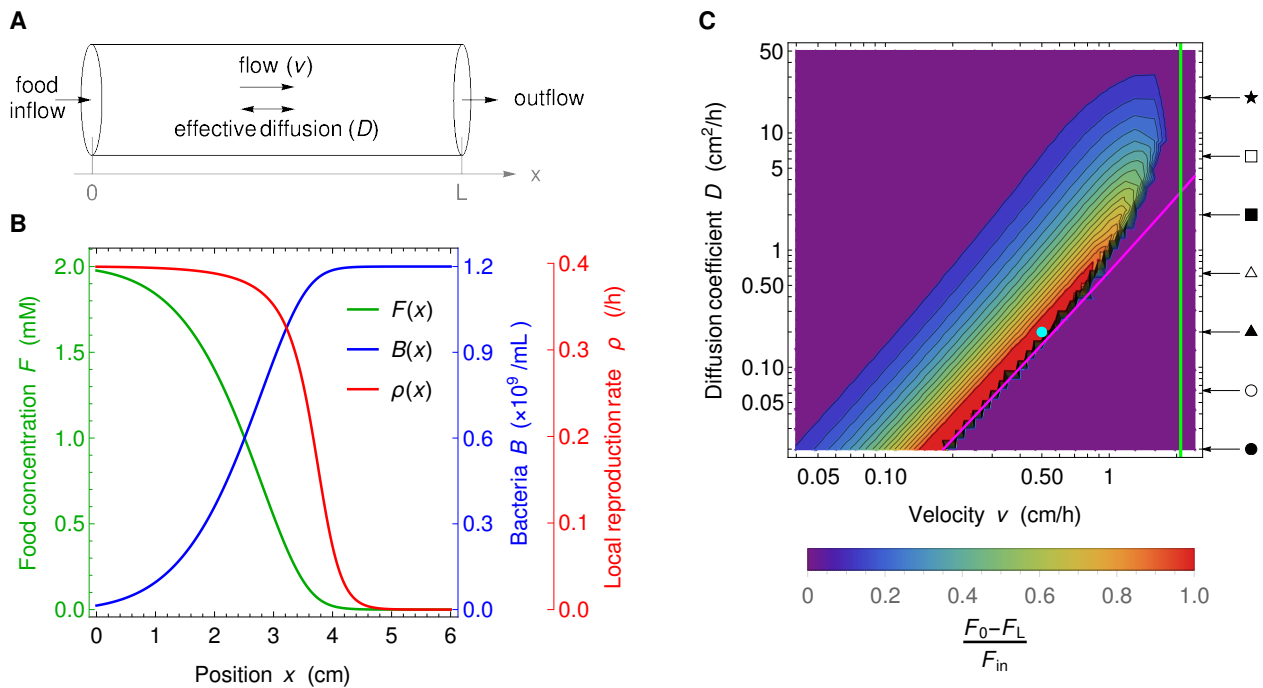
Figure 1: Model of the gut and associated spatial gradients. A: Schematic representation of the gut model investigated. We consider a cylinder with length L and neglect concentration variations in the radial direction, thus simplifying the system to one dimension along the x axis. Transport is modeled as flow with constant velocity v and effective diffusion coefficient D. At the upstream boundary $x = 0$ we consider constant food inflow, and no bacteria inflow, while at the downstream boundary $x = L$ we consider zero diffusive outflow. **B**: Concentration F of food, amount B of bacteria, and reproduction rate ρ of bacteria versus the coordinate x along the gut. Curves are numerical solutions of Eq. 1 for $D = 0.2\,\mathrm{cm^2/h}$, $v = 0.5\,\mathrm{cm/h}$, $k = 0.1\,\mathrm{mM}$, $r = 0.42\,\mathrm{h^{-1}}$, $v F_{\mathrm{in}} = 1\,\mathrm{mM\,cm/h}$, $\alpha = 6.13 \times 10^8\,\mathrm{bacteria/(mL\,mM)}$ and no mutant bacteria. The section area, S, is taken to be $1\,\mathrm{cm^2}$ in the entire paper, and the length L is 6 cm, as in the mini-gut of Ref. [39], in the main text, but is varied in the Supplementary material (see Section S9). The parameters are chosen such that they fall in range of parameters compared to the experiments in [39] and that the concentration profile is dependent of the spatial coordinate. The depicted concentrations represent the state of the system after numerically integrating partial differential Eqs. 1 for time $t = 500\,\mathrm{h}$ which is sufficient to reach the steady state. **C**: Heat map of the level of spatial dependence of the concentration profiles, quantified by $[F(0) - F(L)]/F_{\mathrm{in}}$, versus v and D. High values of $[F(0) - F(L)]/F_{\mathrm{in}}$ (red) mean strong gradients in the gut. Magenta and green lines represent washout limits, resp. $D = v^2(k/F_{\mathrm{in}} + 1)/(4r)$ and $v = rL/(k/F_{\mathrm{in}} + 1)$. Below the magenta line and on the right side of the green line, there are no bacteria in the gut at steady state, while in the purple region on the top left hand side, the system is well-mixed, leading to an almost uniform but non-zero concentration of bacteria in the gut. Parameter values (except v and D) are the same as in panel B. The values of v and D used in panel B are indicated by a circular cyan marker. Arrows and symbols on the right hand-side of the heat map indicate the diffusion coefficient values employed in Figure 4 with the same symbols.

Dynamics and fate of neutral mutants appearing in the gut

Let us now consider neutral mutants that spontaneously appear in the gut at steady state. Mutants may appear at any position along the gut, which can feature strong spatial heterogeneities (see Figure 1). How does the initial position of these mutants affect their dynamics and their steady-state concentration?

The initial local concentration of mutants is assumed to be much smaller than that of the wild type at the position x_{M} where the mutants appear (see Eqs. 3), as we aim to describe the fate of a single mutant or a few mutants, but in the framework of the continuous description of the gut. The early dynamics of mutant concentration is governed by the fluid dynamics in the gut. Indeed, the position x with the highest mutant concentration at a given time t initially follows the $x = x_{\mathrm{M}} + vt$ line, while the time t for which the mutant concentration is maximal for a given position x initially follows the $t = (x - x_{\mathrm{M}})^2/(2D)$ curves (see Supplementary material, Figure S4). This is consistent with the infinite space solution of the diffusion equation obtained from Eqs. 1 when ignoring reproduction. Hence, transport by drift and diffusion allows the early spread of the mutants in the gut. Afterwards, coupling with the reproduction term and the boundary conditions yields more complex dynamics.

Because neutral mutant concentration satisfies the same partial differential equation as wild-type bacteria concentration (see Eqs. 1), the steady-state concentrations of mutant and wild type bacteria satisfy $M(x)/B(x) =$

C, where C depends on the initial conditions but not on x. In other words, the steady-state concentration profile of neutral mutants versus position x along the gut is the same as for wild-type bacteria, but with an overall rescaling. The magnitude of this rescaling (i.e. the value of C) depends on the initial mutant quantity, and on the position x_M where mutant bacteria appear. The latter dependence on x_M is strong in the regime where spatial dependence is strong in the mutant-free system (see Figure 1C), as shown in Figure 2A and Figures S5 and S6 in the Supplementary material. If the number of mutants that appear is held constant, then mutants make up a much larger steady-state fraction of bacteria if they appeared close to the entrance of the gut than if they appeared close to its exit, because they have more opportunity to spread and divide in the gut.
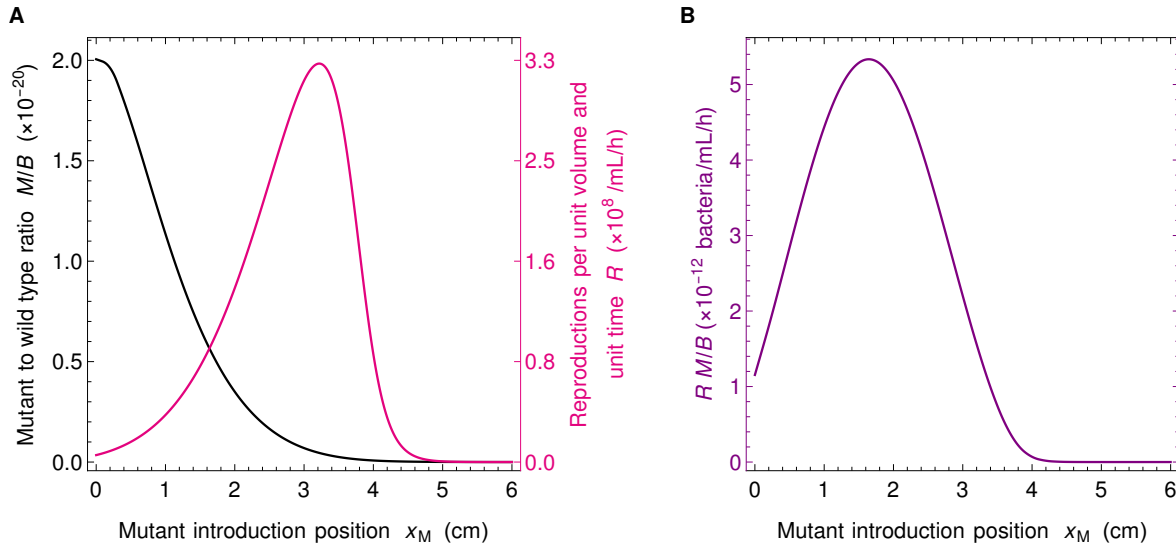

Figure 2: Fate of neutral mutants appearing at various locations in the gut. A: Steady-state ratio M/B of mutant to wild-type bacteria concentrations, and number of reproduction events R per unit volume and unit time versus position x_M of the mutant introduction. The ratio M/B yields the fixation probability of a mutant that appears at a given position x_M in the system. As mutants generally appear upon division, the appearance of new mutants is proportional to R, which thus also matters for the overall likelihood that a mutant appears and fixes. Mutants are introduced at numerical integration time $t = 500\,\text{h}$, when steady state is reached. **B**: Product of the ratio M/B and the number R of reproductions per unit volume and unit time versus x_M. This quantity yields the fixation probability of a mutant that appears proportionally to reproduction rate. Parameter values are the same as in Figure 1B, and F and B are initially at steady state as in Figure 1B, while mutants are introduced locally by using the initial condition in Eqs. 3, with a total number $N_M = 3.33 \times 10^{-11}$ of mutants introduced in the system.

In our deterministic continuous description, bacterial species or strains coexist forever (except in the washout case where they are all wiped away), reflected by the fact that M/B is nonzero at steady state. However, the fate of individual mutants is in fact affected by demographic fluctuations known as genetic drift [42], so that in a finite system, mutants eventually either take over the population or disappear. Here, on a short time scale, mutants either reach deterministic steady state in coexistence with the wild-type, or they get extinct stochastically. If they reach steady state, then, on a longer time scale, proportional to population size [42], one of the two types takes over. What is the probability that a mutant lineage that has reached steady state then fixes in the population? In a well-mixed system, the fixation probability of a neutral mutant is given by the ratio of the number of mutants to the total number of individuals [42]. In our gut model, the steady-state ratio M/B is independent of x in the deterministic limit (note that throughout we have $M \ll B$ so that here $M/(M + B) \approx M/B$, and we only discuss M/B). Moreover, in Eqs. 1, the only non-linearity in the evolution of B and M comes from the dependence of F on B and M. Here, since we introduce a very small amount of mutants, $M_0 \ll B$, when B is at stationary state, and since the overall bacterial population is very large, F remains almost constant through the evolution of M, which entails that the equations for B and M are then approximately linear. Because in the linear case, the equations on averages across replicates of a stochastic system coincide with those of the deterministic large-size limit [48], the fixation probability of neutral mutants in the stochastic case is given by the deterministic steady-state ratio $M/(M + B) \approx M/B$. Given the dependence of this ratio on the initial position x_M of the mutants (see Figure 2A and discussion above), mutants appearing close to the entrance of the gut are much more likely to fix than those appearing close to its exit, in the regime with strong spatial dependence (see Figure 1C).

Where in the gut do the mutants that fix originate? To address this question, we need to account for the apparition of mutants as well as for their fixation. Assume that mutations occur upon division, which is the

case for replication errors. Then, mutants appear at a position x_M proportionally to the local number

$$R(x_M) = B(x_M)\rho(x_M) \tag{6}$$

of reproduction events per unit volume and unit time (where the reproduction rate ρ is given by Eq. 5). This number is small close to the exit of the gut because food is exhausted, but it is also small close to its entrance because bacteria are scarce, and it features a maximum at an intermediate location (see Figure 2A). What ultimately sets the location where mutants that fix tend to originate is the product of M/B and R, whose dependence on the mutant initial position x_M is depicted in Figure 2B. It features a strong spatial dependence, with a maximum at an intermediate position in the gut. In the Supplementary material section S7, we study R and $R\,M/B$ for various parameter values, and show that this maximum of $R\,M/B$ at an intermediate position in the gut is obtained robustly in the regime with strong spatial dependence (see Figure S7).

Spatial structure in the gut increase the fixation probability of neutral mutants

What is the overall probability $\mathcal{F}$ that neutral mutants fix in the gut, averaged over their possible positions of origin? It can be expressed as the integral over all possible initial mutant locations x_M of the fixation probability given x_M, multiplied by the probability that the mutant originates at this location x_M:

$$\mathcal{F} = \frac{\int_0^L R(x_M)\frac{M(x_M)}{B(x_M)}dx_M}{\int_0^L R(x_M)dx_M}. \tag{7}$$

How is the overall fixation probability $\mathcal{F}$ of a neutral mutant affected by the spatial dependence of food and bacterial concentrations in the gut? To address this question, Figure 3 depicts $\mathcal{F}$ versus total population size $N_T = S\int_0^L B(x)dx$ for different velocities v and diffusion coefficients D. In order to include concentration profiles with different degrees of spatial dependence, quantified by $[F(0) - F(L)]/F_{in}$ (see Figure 1C), several values of D were chosen, and for each of them, a range of velocities v was chosen using Figure 1C so that it includes flat profiles for small velocities, spatial profiles for intermediate velocities, and again flat profiles close to the washout limit. Throughout, the food inflow $v\,F_{in}$ at the entrance of the gut was held constant to allow comparison. In a well-mixed system, we would have $\mathcal{F} = N_M/N_T$, where N_M denotes the initial number of mutants in the system and N_T the total number of bacteria in the system [42]. We find an excellent agreement with this expectation in the case of flat concentration profiles. This is evident for small N_T values, which correspond to the largest velocities considered and thus to the washout limit, when the concentration profiles are the flattest (see Figure 3). Conversely, in the strongly spatial regime (red symbols in Figure 3), the fixation probability deviates from the well mixed system expectation, becoming substantially larger than it, and almost independent of the total population. For large N_T, which corresponds to small velocities, and hence flat profiles again, the fixation probability slowly converges back to the well-mixed system expectation (see Figure 3).
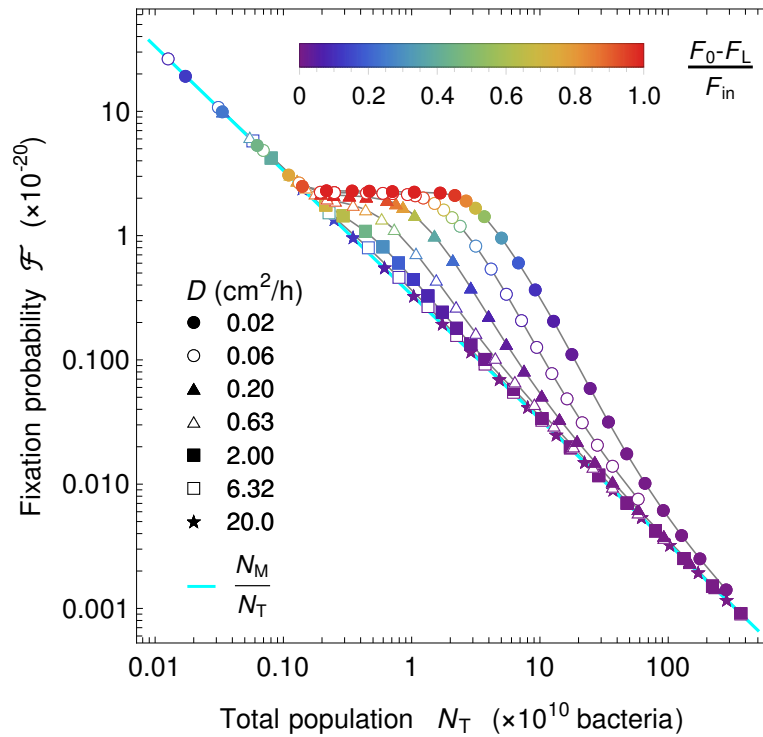
Figure 3: Fate of a neutral mutant versus population size in the gut. Fixation probability $\mathcal{F}$ of mutants appearing proportionally to reproduction rate is shown versus total population size N_{T}, for different diffusion coefficients D (see corresponding markers on the right hand-side of the heat map in Fig. 1C). Markers are colored by the level of spatial dependence of the concentration profiles, quantified by $[F(0) - F(L)]/F_{\mathrm{in}}$ as in Fig. 1C. For strong spatial dependence (red), a plateau is observed, evidencing a large difference with the well-mixed expectation $\mathcal{F} = N_{\mathrm{M}}/N_{\mathrm{T}}$. For each value of D, v is varied while keeping $v\,F_{\mathrm{in}}$ constant, and fixation probability is calculated from Eq. 7 and total population by integrating the sum of the mutant and the wild type in the total space (volume). Parameter values: $D \in [0.02, 20.0]$ cm^2/h, $v \in [0.001, 2.4]$ cm/h, $k = 0.1$ mM, $r = 0.42\,\mathrm{h}^{-1}$, $v\,F_{\mathrm{in}} = 1\,\mathrm{mM\,cm/h}$, and $\alpha = 6.13 \times 10^8$ bacteria/(mL mM) and initial conditions as in Figure 2.

The fixation probability of neutral mutants results from an active population

Why is the fixation probability of neutral mutants larger in the gut in the presence of strong spatial dependence than in a well-mixed population with the same size? An important difference is that not all bacteria are actively reproducing in the gut, while they all have the same replication rate in a well-mixed population. More precisely, in the regime with strong spatial dependence, most replications occur in the region such that the local number of reproduction events $R(x)$ per unit volume and unit time (see Eqs. 6 and 5) is substantial, i.e. visually, under the local replication rate curve, which coincides with the zone where bacterial concentration increases (see Figure 4A). Quantitatively, we define the "active population", i.e. the region with active reproduction, by comparing the replication rate to its maximum possible value, see Figure 4A and the Supplementary material Section S8 for details.

Can the active population, smaller than the total population, and comprising the reproducing bacteria, quantitatively explain the fixation probability observed in the gut in the presence of strong spatial dependence? In order to assess this, we set out to significantly change active population size, and thus the total number of reproduction events, by varying the food inflow $v\,F_{\mathrm{in}}$ at the entrance of the gut, while holding the diffusion coefficient constant at $D =0.02$ cm/h. We took several velocity values, but only retained those such that concentration profiles were strongly spatially dependent. Figure 4B shows the fixation probability $\mathcal{F}$ versus the size N_{A} of the active population in this spatial regime. Our results agree very well with the relation

$$\mathcal{F} = \frac{N_{\mathrm{M}}}{N_{\mathrm{A}}}, \tag{8}$$

where N_{M} is the initial number of mutant bacteria. This corresponds to the well-mixed expectation for the fixation probability of N_{M} mutants in a population of N_{A} bacteria, which confirms that the active population is the one that matters for the process of mutant fixation. This explains why the fixation probability is higher in the spatial system than in the well-mixed one.
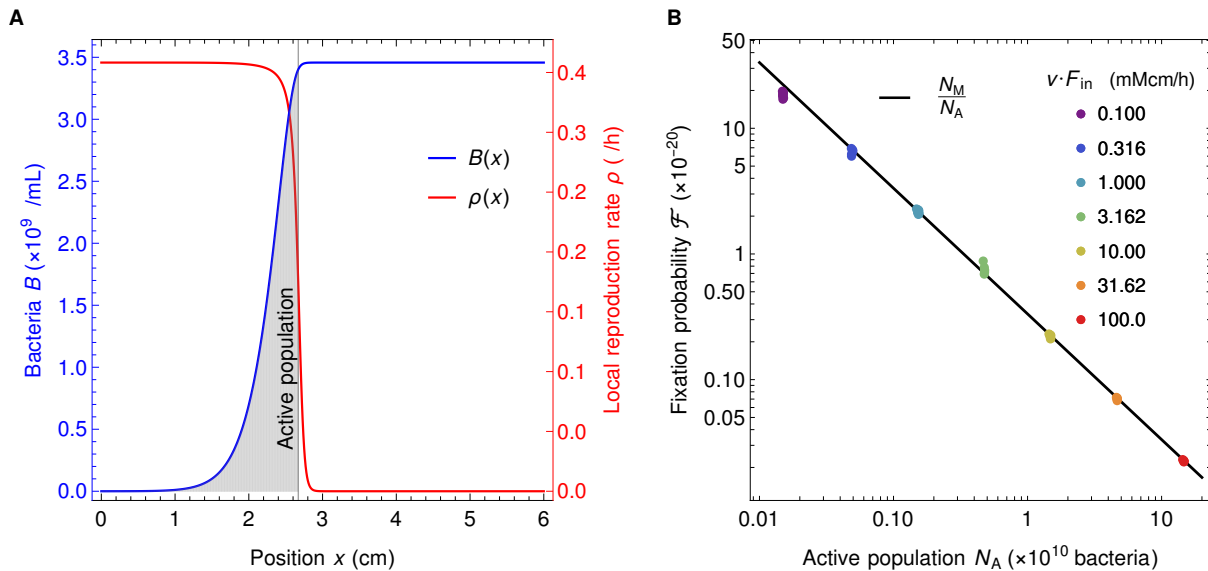
Figure 4: Active population explains the behavior of neutral mutant fixation probability in the gut. A: The active bacterial population (gray shaded area) is defined as the total number of bacteria between the points $x = 0$ and $x = x^*$, where x^* is defined as $F(x^*) = k$, so that $B(x^*) = \alpha F_{\text{in}}(1 - k/F_{\text{in}})$. This corresponds to the region where bacteria have significant reproduction rates. Parameters are $v F_{\text{in}} = 1 \,\text{mM cm/h}$, $v = 0.181 \,\text{cm/h}$, $D = 0.02 \,\text{cm}^2/\text{h}$, $k = 0.1 \,\text{mM}$, $r = 0.42 \,\text{h}^{-1}$, and $\alpha = 0.613 \times 10^9$ bacteria/(mL mM). **B**: Fixation probability $\mathcal{F}$ of neutral mutants in the gut in the regime with strong spatial dependence versus active population N_A, for different values of food inflow $v F_{\text{in}}$ (different colors). Each set of markers with a given color contains between 6 and 11 different points (often overlapping). Diffusion coefficient is the same for all points, $D = 0.02 \,\text{cm}^2/\text{h}$, velocities are $v \in [0.135, 0.171]$ cm/h, $v \in [0.14, 0.18]$ cm/h, $v \in [0.15, 0.185]$ cm/h, $v \in [0.15, 0.181]$ cm/h, $v \in [0.15, 0.186]$ cm/h, $v \in [0.155, 0.182]$ cm/h, $v \in [0.165, 0.186]$ cm/h for $v F_{\text{in}} = 0.1$ to 100.0 mM cm/h, respectively. Other parameters and initial conditions are as in Figure 3. Only the data points satisfying $[F(0) - F(L)]/F_{\text{in}} > 0.9$ are retained, ensuring that we focus on the plateau of the fixation probability with respect to the total population (see Fig. 3). The black line corresponds to $\mathcal{F} = N_M/N_A$. Panel A corresponds to one of the green dots in panel B.

In the Supplementary material, section S9, we demonstrate the generality of the conclusions obtained here by systematically investigating the three dimensionless parameters that fully describe the stationary state of the system (see Figure S8). We demonstrate that the range of these parameters considered in the present study matches the realistic one in the human colon, and we show that Eq. 8 holds in all cases considered, provided that the food concentration profile is strongly spatial (see Figures S10, S9 and S11).

Discussion

We addressed bacterial evolution in the gut within a minimal model that incorporates flow and gradients of food and bacterial concentrations along the gut. We focused on the colon lumen, where the vast majority of our microbiota is located, and we considered neutral mutants appearing in the gut. The dynamics of bacteria and food was described using a system of partial differential equations based on Refs. [39, 40]. In the long term, in a finite-size system, mutants either disappear or take over due to stochastic fluctuations, and the stationary proportion of mutants in our continuous and deterministic description gives their fixation probability. We demonstrated that, in the regime where the profiles of food and bacterial concentrations are strongly spatial, with abundant food and few bacteria upstream, and vice-versa downstream, the stationary concentration of mutants is higher if they start upstream. However, for mutations occurring at replication, the small upstream concentration of bacteria means that few mutants appear there. Accordingly, we found that successful mutants are more likely to originate from an intermediate position along the gut. We studied the overall long term mutant proportion for neutral mutants appearing spontaneously upon division, which also gives their fixation probability. We found that in the almost well-mixed regime, it is given by the ratio of the initial number of mutants to the total bacterial population size, consistently with the well-mixed expectation. By contrast, when the profiles of food and bacterial concentrations are strongly spatial, which is the relevant regime in the gut [39, 40], this fixation probability becomes substantially larger than the well-mixed expectation. Thus, the spatial structure of the gut favors the spread of neutral mutants and the evolution of the population composition. Furthermore, we rationalized this increase of the fixation probability by demonstrating that it stems from the fact that only a subset of the bacterial population is actively replicating. This active population is located upstream, where there is enough food to allow substantial replication. It gives an effective population

size [12, 42] for the fixation of neutral mutants in the complex structured population of the gut.

Studies addressing the impact of spatial population structure on evolution generally consider discrete patches of population with migrations between them, and the same environment in each of them [5–21]. While complex population structures with asymmetric migrations can impact the fixation probabilities of beneficial and deleterious mutants [13, 14, 21], that of neutral mutants appearing uniformly in the population, e.g. upon division, is unaffected [14, 21]. Similarly, chaotic hydrodynamic flow has been predicted to impact non-neutral mutant fixation probabilities, but not neutral ones [49]. In the gut, the flow can be viewed as yielding asymmetric migrations. Strikingly, we found that the fixation probability of neutral mutants could strongly differ from the well-mixed case. Aside the fact that the gut is a continuous system, a crucial difference with the above-cited models of population structure is that, due to directional hydrodynamic flow, the environment varies along the gut, in particular the food and bacterial concentrations, and thus the bacterial division rate. Environmental gradients can strongly impact evolution; for instance, gradients of antibiotics can increase the speed at which antibiotic resistance emerges [32–35]. The coupling of bacterial concentration gradients due to antibiotics with convective flow also has complex implications on evolution [50]. Hydrodynamic flow itself can strongly impact fixation probabilities and fixation times, as has been shown in the case of compressible flows relevant for large-scale turbulent systems such as bacterial populations living at the surface of oceans [29–31]. In these situations, flow reduces the effective population size for fixation probability, and microorganisms born near a flow source are more likely to fix than those born in a flow sink [31]. Albeit obtained in a different hydrodynamic regime, these results share similarities with ours, and together, they demonstrate that hydrodynamic flow, and in particular convective flow, can strongly impact evolution at various scales, from the gut to the ocean.

In addition to hydrodynamic flow and gradients, the gut comprises an upstream zone with few bacteria and rapid growth. This is reminiscent of expanding fronts in populations that invade a new environment [51, 52], which feature reduced competition and reduced effective population sizes, with important consequences on evolution [53–55]. In these cases, the dynamics is different depending on whether the Fisher waves [56] characterizing expansion are driven by the leading edge (pulled) or by the bulk of the wave (pushed) [52] or intermediate (semi-pushed) [57]. Stochasticity has major impacts in the pulled and semi-pushed cases, due to the small numbers of bacteria at the edge [57]. Accordingly, the continuous model we employed may not be adequate for the small numbers of bacteria upstream in the gut. Similarly to models on expanding fronts, we find that mutants appearing upstream are more likely to fix. However, contrary to population expansion on solid substrates [51], the gut features directional hydrodynamic flow. Specifically, bacteria take at least 20 minutes to replicate (here we took a typical replication time of 100 minutes), and since they are transported with the flow, the lineage of an upstream bacteria will be broadly distributed, including where there are many bacteria, before being large enough to affect F sufficiently to modify the dynamical equations via $F/(k + F)$. Thus, the effect of the stochastic front is expected to be small here.

Extending our study from neutral mutants to beneficial and deleterious ones, and studying fixation times and the rate of evolution in the gut, would be interesting topics for future work. Note that given the very large numbers of bacteria at play, fixation is expected to be slow, but even before fixation, our results show that the proportion of mutants is increased by the gut structure compared to a well-mixed system. Furthermore, while the minimal model used here captures some key characteristics of the gut, with a net flow, an effective mixing that is on limited length scales, and a stable bacterial population, the reality of the gut is more complex. In particular, muscle contractions in peristalsis and segmentation [58, 59] mean that the radius of the gut is variable, and yield a complex mixing dynamics. Besides, several food sources and several bacterial species are present, yielding complex ecological dynamics. Bacterial populations in the colon lumen can also interact with those in the mucus and in crypts. In addition, assuming a constant food inflow is a simplification, and in real life food inflow is variable, depending e.g. on the timing of meals, thus adding time variability to the spatial gradients we considered here. Despite all these complications, our results, which can be interpreted simply through the active population, have the potential to be general, and can be tested in more detailed models.

Acknowledgments

References

[1] R. Sender, S. Fuchs, and R. Milo. Revised estimates for the number of human and bacteria cells in the body. *PLoS Biology*, 14(8):e1002533, 2016.

[2] Peter J Turnbaugh, Ruth E Ley, Micah Hamady, Claire M Fraser-Liggett, Rob Knight, and Jeffrey I Gordon. The human microbiome project. *Nature*, 449(7164):804, 2007.

[3] Timothy F Landers, Bevin Cohen, Thomas E Wittum, and Elaine L Larson. A review of antibiotic use in food animals: perspective, policy, and potential. *Public health reports*, 127(1):4–22, 2012.

[4] C Rose, Alison Parker, Bruce Jefferson, and Elise Cartmell. The characterization of feces and urine: a review of the literature to inform advanced treatment technology. *Critical reviews in environmental science and technology*, 45(17):1827–1879, 2015.

[5] S. Wright. Evolution in Mendelian populations. *Genetics*, 16(2):97–159, 1931.

[6] M. Kimura and G. H. Weiss. The Stepping Stone Model of Population Structure and the Decrease of Genetic Correlation with Distance. *Genetics*, 49(4):561–576, Apr 1964.

[7] T. Maruyama. On the fixation probability of mutant genes in a subdivided population. *Genet. Res.*, 15:221–225, 1970.

[8] T. Maruyama. A simple proof that certain quantities are independent of the geographical structure of population. *Theor. Popul. Biol.*, 5(2):148–154, Apr 1974.

[9] T. Nagylaki. The strong-migration limit in geographically structured populations. *J Math Biol*, 9(2):101–114, Apr 1980.

[10] M. Slatkin. Fixation probabilities and fixation times in a subdivided population. *Evolution*, 35(3):477–488, 1981.

[11] N. Barton. The probability of fixation of a favoured allele in a subdivided population. *Genet. Res.*, 62:149–157, 1993.

[12] M. C. Whitlock and N. H. Barton. The effective size of a subdivided population. *Genetics*, 146(1):427–441, May 1997.

[13] M. C. Whitlock. Fixation probability and time in subdivided populations. *Genetics*, 164(2):767–779, Jun 2003.

[14] E. Lieberman, C. Hauert, and M. A. Nowak. Evolutionary dynamics on graphs. *Nature*, 433(7023):312–316, Jan 2005.

[15] Kamran Kaveh, Natalia L. Komarova, and Mohammad Kohandel. The duality of spatial death-birth and birth-death processes and limitations of the isothermal theorem. *Royal Society Open Science*, 2(4):140465, 2015.

[16] Laura Hindersin and Arne Traulsen. Most undirected random graphs are amplifiers of selection for birth-death dynamics, but suppressors of selection for death-birth dynamics. *PLOS Computational Biology*, 11(11):1–14, 11 2015.

[17] Karan Pattni, Mark Broom, Jan Rychtář, and Lara J. Silvers. Evolutionary graph theory revisited: when is an evolutionary process equivalent to the moran process? *Proceedings of the Royal Society A: Mathematical, Physical and Engineering Sciences*, 471(2182):20150334, 2015.

[18] Bahram Houchmandzadeh and Marcel Vallade. The fixation probability of a beneficial mutation in a geographically structured population. *New Journal of Physics*, 13(7):073020, Jul 2011.

[19] B. Houchmandzadeh and M. Vallade. Exact results for fixation probability of bithermal evolutionary graphs. *Biosystems*, 112(1):49–54, Apr 2013.

[20] G. W. Constable and A. J. McKane. Population genetics on islands connected by an arbitrary network: an analytic approach. *J Theor Biol*, 358:149–165, Oct 2014.

[21] L. Marrec, I. Lamberti, and A.-F. Bitbol. Toward a universal model for spatially structured populations. *BioRxiv*, pages 1–24, http://dx.doi.org/10.1101/2020.12.12.422518.

[22] I. Gordo and P. R. A. Campos. Adaptive evolution in a spatially structured asexual population. *Genetica*, 127:217, 05 2006.

[23] L. Perfeito, M. I. Pereira, P. R. Campos, and I. Gordo. The effect of spatial structure on adaptation in Escherichia coli. *Biol. Lett.*, 4(1):57–59, Feb 2008.

[24] S. Kryazhimskiy, D. P. Rice, and M. M. Desai. Population subdivision and adaptation in asexual populations of Saccharomyces cerevisiae. *Evolution*, 66(6):1931–1941, Jun 2012.

[25] R. Korona, C. H. Nakatsu, L. J. Forney, and R. E. Lenski. Evidence for multiple adaptive peaks from populations of bacteria evolving in a structured habitat. *Proc. Natl. Acad. Sci. USA*, 91:9037–9041, 1994.

[26] A. F. Bitbol and D. J. Schwab. Quantifying the role of population subdivision in evolution on rugged fitness landscapes. *PLoS Comput. Biol.*, 10(8):e1003778, Aug 2014.

[27] J. R. Nahum, P. Godfrey-Smith, B. N. Harding, J. H. Marcus, J. Carlson-Stevermer, and B. Kerr. A tortoise-hare pattern seen in adapting structured and unstructured populations suggests a rugged fitness landscape in bacteria. *Proc Natl Acad Sci U S A*, 112(24):7530–7535, Jun 2015.

[28] M. T. France and L. J. Forney. The Relationship between Spatial Structure and the Maintenance of Diversity in Microbial Populations. *Am Nat*, 193(4):503–513, 04 2019.

[29] P. Perlekar, R. Benzi, D. R. Nelson, and F. Toschi. Population dynamics at high Reynolds number. *Phys Rev Lett*, 105(14):144501, Oct 2010.

[30] S. Pigolotti, R. Benzi, M. H. Jensen, and D. R. Nelson. Population genetics in compressible flows. *Phys Rev Lett*, 108(12):128102, Mar 2012.

[31] A. Plummer, R. Benzi, D. R. Nelson, and F. Toschi. Fixation probabilities in weakly compressible fluid flows. *Proc Natl Acad Sci U S A*, 116(2):373–378, 01 2019.

[32] Q. Zhang, G. Lambert, D. Liao, H. Kim, K. Robin, C Tung, N. Pourmand, and R. H. Austin. Acceleration of emergence of bacterial antibiotic resistance in connected microenvironments. *Science*, 333(6050):1764–1767, 2011.

[33] Philip Greulich, Bartłomiej Waclaw, and Rosalind J Allen. Mutational pathway determines whether drug gradients accelerate evolution of drug-resistant cells. *Physical Review Letters*, 109(8):088101, 2012.

[34] R. Hermsen, J. B. Deris, and T. Hwa. On the rapidity of antibiotic resistance evolution facilitated by a concentration gradient. *Proc. Natl. Acad. Sci. USA*, 109:10775–10780, 2012.

[35] Michael Baym, Tami D Lieberman, Eric D Kelsic, Remy Chait, Rotem Gross, Idan Yelin, and Roy Kishony. Spatiotemporal microbial evolution on antibiotic landscapes. *Science*, 353(6304):1147–1151, 2016.

[36] Gregory P Donaldson, S Melanie Lee, and Sarkis K Mazmanian. Gut biogeography of the bacterial microbiota. *Nature Reviews Microbiology*, 14(1):20, 2016.

[37] Ken Kurokawa, Takehiko Itoh, Tomomi Kuwahara, Kenshiro Oshima, Hidehiro Toh, Atsushi Toyoda, Hideto Takami, Hidetoshi Morita, Vineet K Sharma, Tulika P Srivastava, et al. Comparative metagenomics revealed commonly enriched gene sets in human gut microbiomes. *DNA Research*, 14(4):169–181, 2007.

[38] Peter J Turnbaugh, Micah Hamady, Tanya Yatsunenko, Brandi L Cantarel, Alexis Duncan, Ruth E Ley, Mitchell L Sogin, William J Jones, Bruce A Roe, Jason P Affourtit, et al. A core gut microbiome in obese and lean twins. *Nature*, 457(7228):480–484, 2009.

[39] Jonas Cremer, Igor Segota, Chih Yu Yang, Markus Arnoldini, John T. Sauls, Zhongge Zhang, Edgar Gutierrez, Alex Groisman, and Terence Hwa. Effect of flow and peristaltic mixing on bacterial growth in a gut-like channel. *Proc. Natl. Acad. Sci. USA*, 113(41):11414–11419, 2016.

[40] Jonas Cremer, Markus Arnoldini, and Terence Hwa. Effect of water flow and chemical environment on microbiota growth and composition in the human colon. *Proc. Natl. Acad. Sci. USA*, 114(25):6438–6443, 2017.

[41] P. A. P. Moran. Random processes in genetics. *Mathematical Proceedings of the Cambridge Philosophical Society*, 54(1):60–71, 1958.

[42] W. J. Ewens. *Mathematical Population Genetics*. Springer-Verlag, 1979.

[43] Herbert F Helander and Lars Fändriks. Surface area of the digestive tract–revisited. *Scandinavian journal of gastroenterology*, 49(6):681–689, 2014.

[44] Richard A Cone. Barrier properties of mucus. *Advanced drug delivery reviews*, 61(2):75–85, 2009.

[45] Alexander Swidsinski, Jutta Weber, Vera Loening-Baucke, Laura P Hale, and Herbert Lochs. Spatial organization and composition of the mucosal flora in patients with inflammatory bowel disease. *Journal of clinical microbiology*, 43(7):3380–3389, 2005.

[46] Darka Labavić, Claude Loverdo, and Anne-Florence Bitbol. Hydrodynamic flow and concentration gradients in the gut enhance neutral bacterial diversity, (Version v1.0.0), http://doi.org/10.5281/zenodo.4704653. *Zenodo*, 2021.

[47] D. Herbert, R. Elsworth, and R. C. Telling. The continuous culture of bacteria; a theoretical and experimental study. *Microbiology*, 14(3):601–622, 1956.

[48] Leif Gustafsson and Mikael Sternad. When can a deterministic model of a population system reveal what will happen on average? *Mathematical biosciences*, 243(1):28–45, 2013.

[49] F. Herrerías-Azcué, V. Pérez-Muñuzuri, and T. Galla. Stirring does not make populations well mixed. *Sci Rep*, 8(1):4068, 03 2018.

[50] M. Gralka, D. Fusco, S. Martis, and O. Hallatschek. Convection shapes the trade-off between antibiotic efficacy and the selection for resistance in spatial gradients. *Phys Biol*, 14(4):045011, 07 2017.

[51] O. Hallatschek, P. Hersen, S. Ramanathan, and D. R. Nelson. Genetic drift at expanding frontiers promotes gene segregation. *Proc. Natl. Acad. Sci. USA*, 104:19926–19930, 2007.

[52] O. Hallatschek and D. R. Nelson. Gene surfing in expanding populations. *Theor Popul Biol*, 73(1):158–170, Feb 2008.

[53] J. M. Travis, T. Munkemuller, O. J. Burton, A. Best, C. Dytham, and K. Johst. Deleterious mutations can surf to high densities on the wave front of an expanding population. *Mol. Biol. Evol.*, 24(10):2334–2343, Oct 2007.

[54] L. Bosshard, I. Dupanloup, O. Tenaillon, R. Bruggmann, M. Ackermann, S. Peischl, and L. Excoffier. Accumulation of Deleterious Mutations During Bacterial Range Expansions. *Genetics*, 207(2):669–684, 10 2017.

[55] M. Gralka, F. Stiewe, F. Farrell, W. Mobius, B. Waclaw, and O. Hallatschek. Allele surfing promotes microbial adaptation from standing variation. *Ecol. Lett.*, 19(8):889–898, 08 2016.

[56] R. A. Fisher. The wave of advance of advantageous genes. *Ann. Eugenics*, 7:353–369, 1937.

[57] G. Birzu, O. Hallatschek, and K. S. Korolev. Fluctuations uncover a distinct class of traveling waves. *Proc Natl Acad Sci U S A*, 115(16):E3645–E3654, 04 2018.

[58] A. C. Ailiani, T. Neuberger, J. G. Brasseur, G. Banco, Y. Wang, N. B. Smith, and A. G. Webb. Quantitative analysis of peristaltic and segmental motion in vivo in the rat small intestine using dynamic MRI. *Magn Reson Med*, 62(1):116–126, Jul 2009.

[59] J. D. Huizinga and W. J. Lammers. Gut peristalsis is governed by a multitude of cooperating mechanisms. *Am J Physiol Gastrointest Liver Physiol*, 296(1):1–8, Jan 2009.

[60] J. Crank. *The Mathematics of Diffusion*. Oxford science publications. Clarendon Press, 1979.

[61] NI McNeil. The contribution of the large intestine to energy supplies in man. *The American journal of clinical nutrition*, 39(2):338–342, 1984.

[62] JC Debongnie and SF Phillips. Capacity of the human colon to absorb fluid. *Gastroenterology*, 74(4):698–703, 1978.

[63] Karin Kovárová-Kovar and Thomas Egli. Growth kinetics of suspended microbial cells: from single-substrate-controlled growth to mixed-substrate kinetics. *Microbiology and molecular biology reviews*, 62(3):646–666, 1998.

[64] Ivan Ramirez, Eveline IP Volcke, Rajagopal Rajinikanth, and Jean-Philippe Steyer. Modeling microbial diversity in anaerobic digestion through an extended adm1 model. *Water research*, 43(11):2787–2800, 2009.

[65] Alonzo W Lawrence and Perry L McCarty. Kinetics of methane fermentation in anaerobic treatment. *Journal (Water Pollution Control Federation)*, pages R1–R17, 1969.

[66] Sherwood L. Gorbach, Andrew G. Plaut, Laila Nahas, Louis Weinstein, Gunter Spanknebel, and Ruven Levitan. Studies of intestinal microflora: II. microorganisms of the small intestine and their relations to oral and fecal flora. *Gastroenterology*, 53(6):856–867, 1967.

[67] Biomechanics of the digestive system. In Takami Yamaguchi, Takuji Ishikawa, and Yohsuke Imai, editors, *Integrated Nano-Biomechanics*, Micro and Nano Technologies, pages 71–99. Elsevier, Boston, 2018.

[68] JH Cummings, DJ Jenkins, and HS Wiggins. Measurement of the mean transit time of dietary residue through the human gut. *Gut*, 17(3):210–218, 1976.

[69] M Proano, M Camilleri, SF Phillips, GM Thomforde, ML Brown, and RL Tucker. Unprepared human colon does not discriminate between solids and liquids. *American Journal of Physiology-Gastrointestinal and Liver Physiology*, 260(1):G13–G16, 1991.

[70] Beth Gibson, Daniel J Wilson, Edward Feil, and Adam Eyre-Walker. The distribution of bacterial doubling times in the wild. *Proceedings of the Royal Society B*, 285(1880):20180789, 2018.

12

Supplementary material

Contents

S1   Numerical methods

S1.1   Discretization of the partial differential equation system

In order to solve the system 1 numerically, we employ an explicit method using a forward difference for the time derivative at time t and a central difference for the space derivative at position x. Explicitly, the relevant differential operators are replaced by the following expressions:

$$\frac{\partial Y}{\partial t} \to \frac{Y(t,x) - Y(t - \Delta t, x)}{\Delta t}, \tag{9a}$$

$$\frac{\partial Y}{\partial x} \to \frac{Y(t, x + \Delta x) - Y(t, x - \Delta x)}{2\Delta x}, \tag{9b}$$

$$\frac{\partial^2 Y}{\partial x^2} \to \frac{Y(t, x + \Delta x) - 2Y(t,x) + Y(t, x - \Delta x)}{(\Delta x)^2}, \tag{9c}$$

where Δt and Δx represent the discrete steps in time and space, respectively. Here $Y(t,x)$ can represent the concentration of food F, or wild type bacteria B, or mutant bacteria M, at time t and coordinate x.

Substituting the differential operators in Eqs. 1 using Eqs. 9 yields

$$F(t + \Delta t, x) = F(t, x) + D \frac{F(t, x + \Delta x) - 2F(t, x) + F(t, x - \Delta x)}{(\Delta x)^2} \Delta t -$$

$$- v \frac{F(t, x + \Delta x) - F(t, x - \Delta x)}{2\Delta x} \Delta t - \frac{r}{\alpha} (B(t, x) + M(t, x)) \frac{F(t, x)}{k + F(t, x)} \Delta t, \tag{10a}$$

$$B(t + \Delta t, x) = B(t, x) + D \frac{B(t, x + \Delta x) - 2B(t, x) + B(t, x - \Delta x)}{(\Delta x)^2} \Delta t -$$

$$- v \frac{B(t, x + \Delta x) - B(t, x - \Delta x)}{2\Delta x} \Delta t + r B(t, x) \frac{F(t, x)}{k + F(t, x)} \Delta t, \tag{10b}$$

$$M(t + \Delta t, x) = M(t, x) + D \frac{M(t, x + \Delta x) - 2M(t, x) + M(t, x - \Delta x)}{(\Delta x)^2} \Delta t -$$

$$v \frac{M(t, x + \Delta x) - M(t, x - \Delta x)}{2\Delta x} \Delta t + r M(t, x) \frac{F(t, x)}{k + F(t, x)} \Delta t. \tag{10c}$$

The boundary conditions in $x = 0$ from Eqs. 2 become

$$F(t, 0 - \Delta x) = F(t, 0 + \Delta x) + \frac{2\Delta x}{D} v \left[F_{\text{in}} - F(t, 0) \right], \tag{11a}$$

$$B(t, 0 - \Delta x) = B(t, 0 + \Delta x) - \frac{2\Delta x}{D} v B(t, 0), \tag{11b}$$

$$M(t, 0 - \Delta x) = M(t, 0 + \Delta x) - \frac{2\Delta x}{D} v M(t, 0), \tag{11c}$$

while the boundary conditions in $x = L$ from Eqs. 2 become

$$F(t, L + \Delta x) = F(t, L - \Delta x), \tag{12a}$$

$$B(t, L + \Delta x) = B(t, L - \Delta x), \tag{12b}$$

$$M(t, L + \Delta x) = M(t, L - \Delta x). \tag{12c}$$

The spatial discrete step Δx is in general chosen to be 0.01 cm. This value is small enough to ensure convergence for most model parameters, and to have a good spatial resolution for analysis. Note however that for some parameters, the term $[F_{\text{in}} - F(t, 0)]$ in Eq. 11a can be very large which can lead to numerical instability. To compensate, the spatial step, Δx, needs to be reduced. Once Δx is chosen, the value of Δt should satisfy the stability condition $\Delta t \leq (\Delta x)^2/(2D)$ [60]. Specifically, we take $\Delta t = 0.8(\Delta x)^2/(2D)$.

S1.2   Obtaining stationary profiles without and with mutants

Numerically, we determine the unique solution for food concentration that satisfies $F(x) < F_{\text{in}}$ for all x. Thus, the steady-state profile of food concentration is independent of the initial conditions as long as they are all positive. In general, for our numerical integration, we choose initial conditions not too far to the steady state, namely $F(0, x) = F_0 \in (0, F_{\text{in}})$, $B(0, x) = \alpha[F_{\text{in}} - F(0, x)]$, and $M(0, x) \ll B(0, x)$, in order to obtain faster convergence. If there is no mutant bacteria, the steady state of the wild type bacteria concentration is also uniquely defined through the relation $B(x) = \alpha[F_{\text{in}} - F(x)]$. However, if there are both wild type and mutant bacteria in the system, then the steady state solution is uniquely defined only for the total bacterial concentration, while individual concentrations depend on the initial conditions for wild type and mutant bacteria.

In practice, the stationary state in the absence of mutant bacteria is found using Eqs. 10 coded in the Fortran90 programming language (code available at https://doi.org/10.5281/zenodo.4704653 [46]) with homogeneous initial conditions

$$F(0, x) = 0.9 F_{\text{in}}, \tag{13a}$$

$$B(0, x) = \alpha[F_{\text{in}} - F(0, x)] = 0.1\alpha F_{\text{in}}. \tag{13b}$$

The time used in all numerical integrations is $t = 500\,\text{h}$, which is long enough for the system to reach the steady state for all choices of parameters considered in this paper.

To find the mutant concentration profile that is crucial to our calculation of the fixation probability, we consider the system without mutants at steady state, and we assume that mutants appear at one local position, x_{M}, in

the gut segment. We again solve Eqs. 10 for time $t = 500\,\mathrm{h}$, but now with the initial conditions

$$F(0, x) = F^*(0, x), \tag{14a}$$

$$B(0, x) = B^*(0, x), \tag{14b}$$

$$M(0, x) = \begin{cases} M_0, & |x - x_\mathrm{M}| \le \Delta x/2, \\ 0, & |x - x_\mathrm{M}| > \Delta x/2, \end{cases} \tag{14c}$$

where F^* and B^* represent steady state concentrations without mutant bacteria, while $M_0 \ll B(x_M)$ is the initial local mutant concentration. More precisely, denoting by N_M the total number of mutant bacteria introduced in the system, the quantity M_0 is the initial concentration in the segment $[x_\mathrm{M} - \Delta x/2, x_\mathrm{M} + \Delta x/2]$, where Δx is the spatial discrete step of our numerical resolutions. Hence, M_0 satisfies $N_\mathrm{M} M_0 S \Delta x$, where N_M is the total number of mutants introduced in the system. Note that since we are using central difference discretization, we need to double the M_0 value on boundaries of the segment where the mutants are introduced, in order to have the same N_M there as in the rest of the segment. In practice, we choose the value $N_\mathrm{M} = 3.33 \times 10^{-11}$ bacteria, so that for any choice of parameters used in this paper and for any initial mutant position x_M, the relation $M_0 \ll B(x_\mathrm{M})$ is satisfied. Importantly, since the stationary concentration of mutant bacteria is proportional to M_0, all results scale with it, and we are not losing generality by fixing the value of M_0.

S1.3   Conversion between food and bacteria concentrations

The initial unit of food concentration is moles per liter, and that of bacterial concentration is optical density, OD [39], which can be converted to numbers of bacteria per volume by using the calibration curve in [39]. Specifically, the conversion factor we take is $1\,\mathrm{OD} = 3.33 \times 10^9$ bacteria/mL. Then the parameter α allows to convert between food and bacteria concentrations.

Importantly, because α is just a scaling factor, a change in this value will modify the bacterial concentration quantitatively, but the spatial profile and all the other conclusions will remain identical.

S2   Stationary profiles without mutants

S2.1   Ordinary differential equation description

Without mutants, at stationary state, Eq. 1 yields:

$$0 = D\frac{\partial^2 F}{\partial x^2} - v\frac{\partial F}{\partial x} - \frac{r}{\alpha}\frac{FB}{k+F}, \tag{15}$$

$$0 = D\frac{\partial^2 B}{\partial x^2} - v\frac{\partial B}{\partial x} + r\frac{FB}{k+F}, \tag{16}$$

with boundary conditions in Eq. 2.

Introducing $f = \alpha F + B$, we have at stationary state

$$C = D\frac{\partial f}{\partial x} - vf, \tag{17}$$

where C is a constant. The solution reads

$$f(x) = -\frac{C}{v} + C' e^{vx/D}, \tag{18}$$

where C' is a constant. Applying the boundary conditions yields $C' = 0$ and $C = -v\alpha F_\mathrm{in}$. Thus,

$$\alpha F(x) + B(x) = f(x) = \alpha F_\mathrm{in}, \tag{19}$$

and this specific linear combination of B and F is independent from x: food effectively gets converted into bacteria.

Now we can inject this into the equation on F to decouple it from B, yielding:

$$0 = D\frac{\partial^2 F}{\partial x^2} - v\frac{\partial F}{\partial x} - r\frac{F(F_\mathrm{in} - F)}{k+F}, \tag{20}$$

which is a second order nonlinear ordinary differential equation.

15

S2.2   Dimensionless form

Let us make the variable change $s = xv/D$, and let us introduce the function ϕ satisfying $\phi(s = xv/D) = F(x)/F_{\text{in}}$ for all x. We obtain

$$0 = \frac{\partial^2 \phi}{\partial s^2} - \frac{\partial \phi}{\partial s} - \lambda \frac{\phi(1 - \phi)}{\kappa + \phi} \,, \tag{21}$$

which involves the dimensionless numbers

$$\kappa = \frac{k}{F_{\text{in}}} \,, \tag{22}$$

and

$$\lambda = \frac{rD}{v^2} \,. \tag{23}$$

The associated boundary conditions are:

$$\phi(s = 0) - \frac{\partial \phi}{\partial s}(s = 0) = 1 \,, \tag{24}$$

$$\frac{\partial \phi}{\partial s}(s = \sigma) = 0 \tag{25}$$

where

$$\sigma = \frac{Lv}{D} \tag{26}$$

is the third dimensionless number describing the system [39].

S2.3   Some stationary profiles

In practice, the partial differential equations in Eqs. 1 with boundary conditions in Eqs. 2 and initial conditions in Eqs. 3 were solved numerically as explained above. Examples of profiles obtained are given in Figure S1. Note that we checked that the long-term results from their direct resolution was consistent to those obtained by numerically solving the ordinary differential equation 20 giving the stationary state of the system.
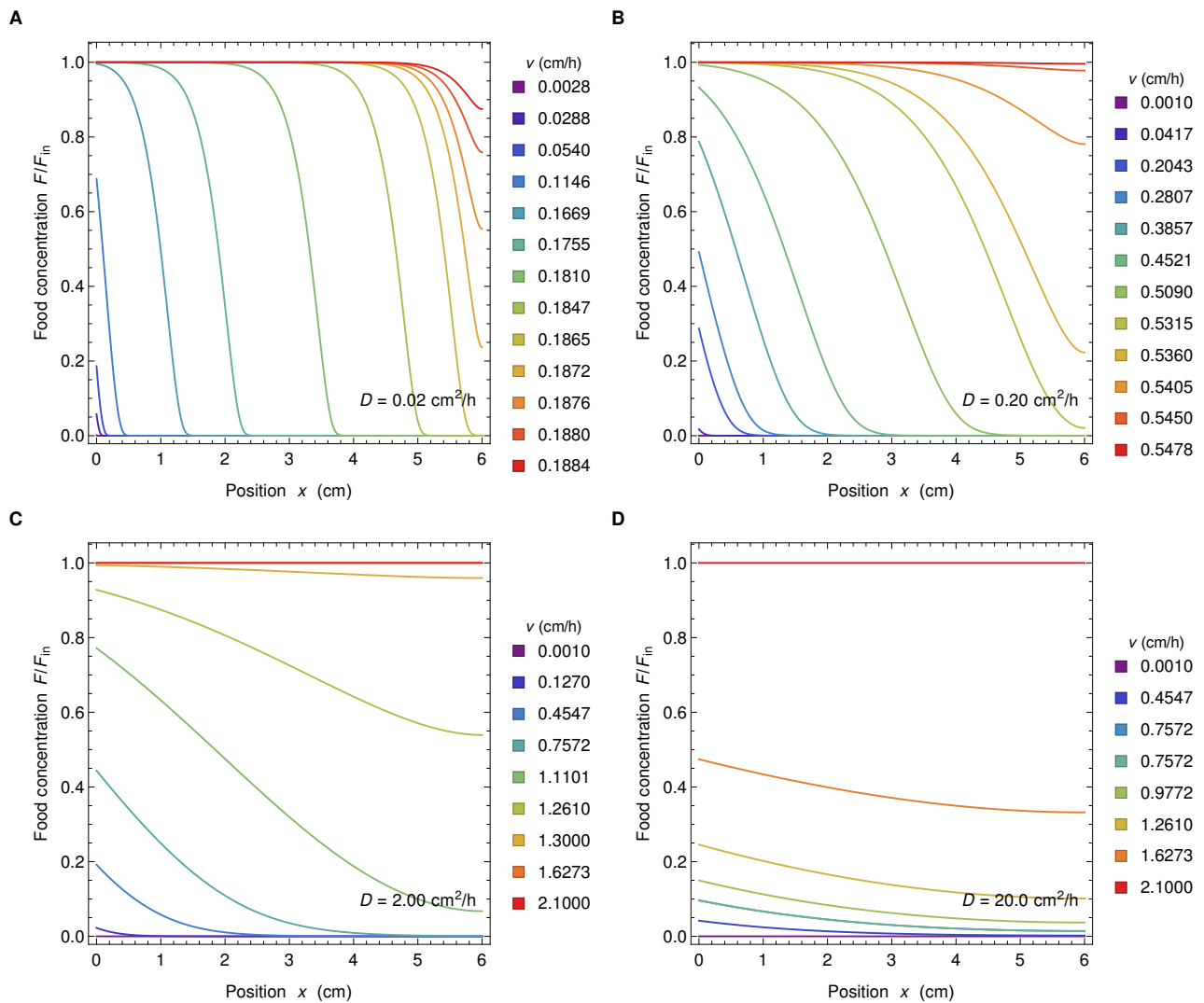
Figure S1: Food concentration profiles. Food concentration F normalized by the food concentration inflow F_{in} versus position x along the gut for four different values of the diffusion coefficient (panels A to D) and several values of velocity (different colors in each panel). Values of diffusion coefficients and velocity are indicated in each panel. Other parameter values are $k = 0.1\,\mathrm{mM}$, $r = 0.42\,\mathrm{h}^{-1}$, $v\,F_{in} = 1\,\mathrm{mM\,cm/h}$, $\alpha = 6.13 \times 10^8\,\mathrm{bacteria/(mL\,mM)}$.

S3 Washout limits

The washout limits are the limits where all bacteria get washed out of the system. Mathematically, they correspond to a bifurcation point in the parameter space where the trivial steady state solution $F(x) = F_{\text{in}}$ (and $B(x) = 0$) becomes stable.

In the chemostat, this limit is easy to determine. There are two steady state solutions, $F^c = kc/(r - c)$ and $F^* = F_{\text{in}}^c$. Eigenvalues of the Jacobian associated to Eqs. 35 and 36 for both steady states change their sign at same point in the parameter space, namely at

$$c = \frac{r}{k/F_{\text{in}}^c + 1} \equiv c_{\text{wo}}. \tag{27}$$

The bifurcation scenario is such that at c_{wo} the two steady state solutions collide, change stability, and one (nontrivial) solution disappears, making it a transcritical bifurcation.

In the spatial system, the bifurcation analysis is not analytically easy. Numerically, we can determine a similar scenario. We find one positive nontrivial solution for $v < v_{\text{wo}}$, where v_{wo} is the bifurcation point which depends on the rest of the system parameters, and only the trivial solution for $v > v_{\text{wo}}$, implying a change of the stability at $v = v_{\text{wo}}$ when the two steady states collide.

It is nevertheless possible to find analytical estimates for the washout limits in the spatial system, as discussed in Ref. [39]. Let us first consider the case of large diffusion coefficients, when concentration profiles are flat regardless of the value of v. We compare the time τ_{flow} needed for a bacterium to travel through the system from the entrance to the exit to the minimal time τ_{repl} taken by a bacterium to replicate in this system (for $F = F_{in}$). If $\tau_{\text{flow}} < \tau_{\text{repl}}$, i.e.

$$\frac{L}{v} < \frac{\kappa + 1}{r}, \tag{28}$$

bacteria get washed out, so that an estimate of the washout velocity is

$$v_{\text{wo}} = \frac{rL}{\kappa + 1}, \tag{29}$$

which is in good agreement with the numerical results, as shown by Figure S2, and Figure 1C in the main text.

Next, let us compare the diffusion and flow characteristic lengths at the time of replication, τ_{repl}. Washout occurs if $L_{\text{diff}} < L_{\text{flow}}$, i.e.

$$\sqrt{2D\tau_{\text{repl}}} < v\tau_{\text{repl}}, \tag{30}$$

$$\sqrt{2\frac{D(\kappa + 1)}{r}} < \frac{v(\kappa + 1)}{r}, \tag{31}$$

which gives

$$v_{\text{wo}} = \sqrt{\frac{2rD}{\kappa + 1}}. \tag{32}$$

This second washout limit is in agreement with the numerical results depicted in Figures S2 and 1 up to a factor 2. Indeed, numerically, we find a good agreement with

$$v_{\text{wo}} = \sqrt{\frac{4rD}{\kappa + 1}}. \tag{33}$$

The results in Figure S2 are consistent with those of Figure 1C where $(\kappa + 1) \leq 1.25$, and demonstrate the robustness of these results across a wide range of κ values.
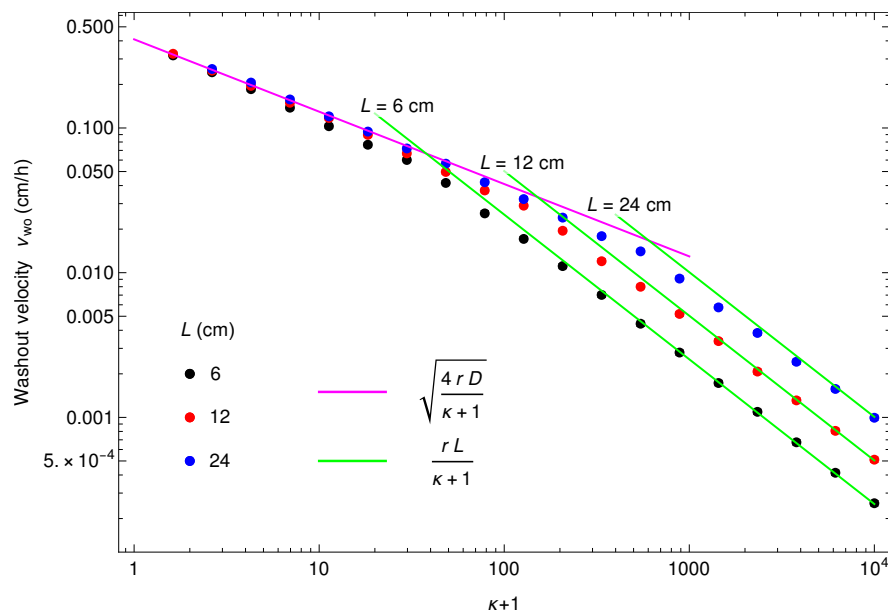
Figure S2: Washout limits in the spatial system as a function of $\kappa + 1$. The two washout limits are obtained by fixing the diffusion coefficient at $0.1\,\mathrm{cm}^2/\mathrm{h}$, and varying the velocity for 20 different values of $\kappa + 1$. The first velocity for which $F(L) > 1. - 10^{-10}$ is recorded as the washout velocity v_{wo}. The process is repeated for three different values of length $L = 6, 12, 24$ cm. Other parameters are $v\,F_{\mathrm{in}} = 1\,\mathrm{mM\,cm/h}$, $k = \kappa F_{\mathrm{in}}$ mM, $r = 0.42\,\mathrm{h}^{-1}$, $\alpha = 6.13 \times 10^8$ bacteria/(mL mM). The green and magenta lines correspond to the two washout limits described by Eqs. 29 and 33, respectively.

19

S4 Correspondence between the spatial system and the chemostat

S4.1 Main matching condition

We wish to match the total number of divisions occurring in the spatial system and in the chemostat. At stationary state we thus aim to match the amount of food entering and exiting these different systems, as well as the amount of bacteria exiting them.

- Spatial system: amount of food entering: $dN_{\mathrm{F,in}}/dt = F_{\mathrm{in}}vS$; amount of food exiting: $dN_{\mathrm{F,out}}/dt = F(L)vS$; amount of bacteria exiting: $dN_{\mathrm{B,out}}/dt = B(L)vS$;

- Chemostat: amount of food entering: $dN_{\mathrm{F,in}}/dt = F_{\mathrm{in}}^{\mathrm{c}}cV$; amount of food exiting: $dN_{\mathrm{F,out}}/dt = F^{\mathrm{c}}cV$; amount of bacteria exiting: $dN_{\mathrm{B,out}}/dt = B^{\mathrm{c}}cV$.

Here V is the volume of the chemostat, c is the dilution rate i.e. the outflow rate per unit volume of the chemostat. Concentrations in the chemostat are indicated by a superscript c. Meanwhile, v denotes the velocity in the spatial system, S the section and L the length of the spatial system.

Hence, our matching condition reads:

$$\frac{F_{\mathrm{in}}}{F_{\mathrm{in}}^{\mathrm{c}}} = \frac{F(L)}{F^{\mathrm{c}}} = \frac{B(L)}{B^{\mathrm{c}}} = \frac{cV}{vS}. \tag{34}$$

S4.2 Constraints from each separate system

In the spatial system, we have $F(L) = F_{\mathrm{in}}\phi(\kappa, \lambda, \sigma)$ and $B(L) = \alpha\left[F_{\mathrm{in}} - F(L)\right]$, i.e. $B(L) = \alpha F_{\mathrm{in}}\left[1 - \phi(\kappa, \lambda, \sigma)\right]$, where ϕ is the dimensionless function introduced above.

In the chemostat, the following equations are satisfied:

$$\frac{dF^{\mathrm{c}}}{dt} = -\frac{r}{\alpha}\frac{F^{\mathrm{c}}B^{\mathrm{c}}}{k + F^{\mathrm{c}}} + cF_{\mathrm{in}}^{\mathrm{c}} - cF^{\mathrm{c}}, \tag{35}$$

$$\frac{dB^{\mathrm{c}}}{dt} = r\frac{F^{\mathrm{c}}B^{\mathrm{c}}}{k + F^{\mathrm{c}}} - cB^{\mathrm{c}}. \tag{36}$$

At stationary state

$$0 = -\frac{r}{\alpha}\frac{F^{\mathrm{c}}B^{\mathrm{c}}}{k + F^{\mathrm{c}}} + cF_{\mathrm{in}}^{\mathrm{c}} - cF^{\mathrm{c}}, \tag{37}$$

$$0 = r\frac{F^{\mathrm{c}}B^{\mathrm{c}}}{k + F^{\mathrm{c}}} - cB^{\mathrm{c}}. \tag{38}$$

If $B^{\mathrm{c}} \neq 0$, this yields $rF^{\mathrm{c}}/(k + F^{\mathrm{c}}) = c$, which means that the dilution rate c of the chemostat sets the effective division rate of the bacteria, a fundamental chemostat property. And then (with $c \neq 0$)

$$F^{\mathrm{c}} = \frac{kc}{r - c}, \tag{39}$$

$$B^{\mathrm{c}} = \alpha\left(F_{\mathrm{in}}^{\mathrm{c}} - F^{\mathrm{c}}\right) = \alpha F_{\mathrm{in}}^{\mathrm{c}}\left(1 - \frac{k}{F_{\mathrm{in}}^{\mathrm{c}}}\frac{c}{r - c}\right). \tag{40}$$

Hence, our matching condition Eq. 34 reads:

$$\frac{F_{\mathrm{in}}}{F_{\mathrm{in}}^{\mathrm{c}}} = \frac{F_{\mathrm{in}}\phi(\kappa, \lambda, \sigma)}{kc/(r - c)} = \frac{\alpha F_{\mathrm{in}}\left[1 - \phi(\kappa, \lambda, \sigma)\right]}{\alpha F_{\mathrm{in}}^{\mathrm{c}}\left[1 - k/F_{\mathrm{in}}^{\mathrm{c}}\,c/(r - c)\right]} = \frac{cV}{vS}, \tag{41}$$

which reduces to two equations relating the spatial system (left hand-side) to the chemostat (right hand-side):

$$\phi(\kappa, \lambda, \sigma) = \frac{k}{F_{\mathrm{in}}^{\mathrm{c}}}\frac{c}{r - c}, \tag{42}$$

$$vSF_{\mathrm{in}} = cVF_{\mathrm{in}}^{\mathrm{c}}. \tag{43}$$

We assume that the parameters of the spatial system are given. Then we need to choose those of the chemostat in order to have a good matching. The parameters specific to the chemostat are $c, F_{\mathrm{in}}^{\mathrm{c}}, V$. Note that k and r are assumed to be the same in both systems. In principle Eqs. 42 and 43 allow us to fix 2 out of these 3 free chemostat parameters.

S4.3   Additional matching conditions

We may want to impose additional matching conditions between the chemostat and the spatial system:

1. Same total volume: $V = SL$. This implies $\frac{cV}{vS} = \frac{cL}{v}$, and Eq. 34 would be modified accordingly.

2. Same volume exiting per unit time: $cV = vS$. This implies $\frac{cV}{vS} = 1$, and Eq. 34 would be modified accordingly.

3. Same outflow rate relative to the total volume: $c = \frac{vS}{LS} = \frac{v}{L}$. This implies $\frac{cV}{vS} = \frac{V}{LS}$, and Eq. 34 would be modified accordingly.

We note that if we impose two of these three conditions simultaneously, then the third one is also satisfied automatically, but Eqs. 42 and 43 and all three conditions above can be satisfied simultaneously only when $F(L) = vk/(rL - v)$.

S4.4   Properties of the matching chemostats

In general, we can impose only 3 independent conditions, setting the values of $c, F_{\text{in}}^{\text{c}}, V$. Specifically, we have to take Eqs. 42 and 43, plus one of the three conditions numbered 1, 2 and 3 above. These three possibilities are discussed in Table S1 and illustrated in Figure S3.

Matching condition		c	F_{in}^{c}	V
1. Same total volume	$\frac{cV}{vS} = \frac{cL}{v}$	$\frac{F(L)v}{2Lk}\left(\sqrt{\frac{4Lrk}{F(L)v}+1}-1\right)$	$\frac{F_{\text{in}}v}{2Lr}\left(1+\sqrt{\frac{4Lrk}{F(L)v}+1}\right)$	$L\,S$
2. Same volume exiting per unit time	$\frac{cV}{vS} = 1$	$\frac{F(L)r}{k+F(L)}$	F_{in}	$\frac{v\,S(F(L)+k)}{F(L)r}$
3. Same outflow rate relative to the total volume	$\frac{cV}{vS} = \frac{V}{SL}$	$\frac{v}{L}$	$\frac{F_{\text{in}}kv}{F(L)(Lr-v)}$	$\frac{F(L)\,L\,S(Lr-v)}{kv}$

Table S1: Chemostat parameters $c, F_{\text{in}}^{\text{c}}, V$ as a function of the parameters of the spatial system for three different matching conditions.
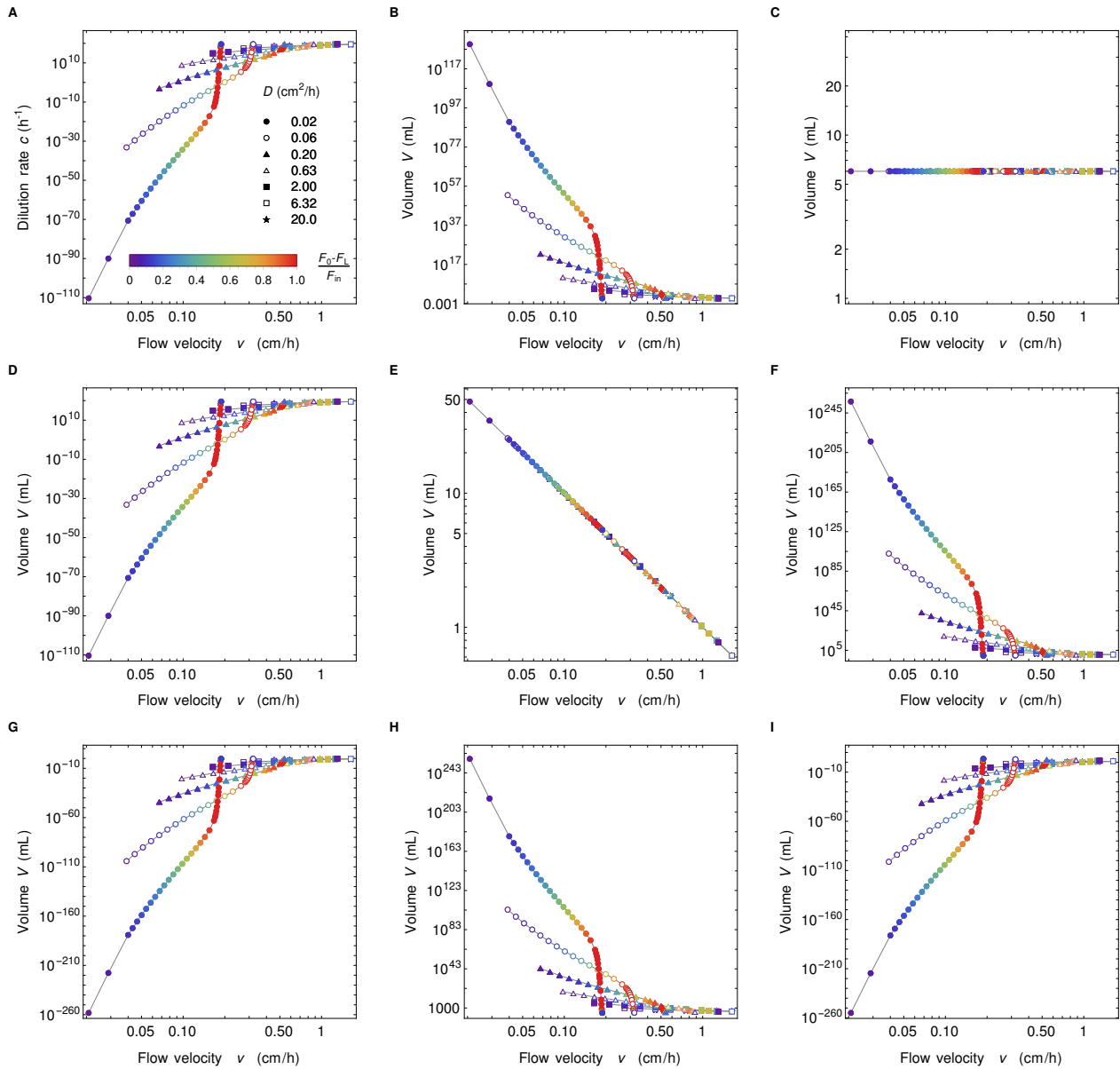
Figure S3: Chemostat parameters. Parameters of the chemostat matching the spatial system in the conditions of Figure 3. Each row in the figure (top to bottom) represents matching condition 1 to 3, while each column in the figure represents a given parameter: dilution rate c (left), food inflow F_{in}^c (middle), and volume V (right). Due to the very small values of food concentration exiting the gut, parameters of the chemostat system can have very large or very small values. This is particularly true for smaller diffusion constants and/or small velocities.

Finally, table S2 gives the expression of various useful quantities for the spatial system and for the chemostat.

	Spatial system	Chemostat
Reproduction rate	$\rho(x) = r\dfrac{F(x)}{k + F(x)}$	$\rho^{\mathrm{c}} = r\dfrac{F^{\mathrm{c}}}{k + F^{\mathrm{c}}}$
Reproductions per unit volume and unit time	$R(x) = B(x)\rho(x)$ $= r\alpha\dfrac{F(x)\left[F_{\mathrm{in}} - F(x)\right]}{k + F(x)}$	$R^{\mathrm{c}} = B^{\mathrm{c}}\rho^{\mathrm{c}}$ $= r\alpha\dfrac{F^{\mathrm{c}}\left(F^{\mathrm{c}}_{\mathrm{in}} - F^{\mathrm{c}}\right)}{k + F^{\mathrm{c}}}$
Total reproduction rate	$N_{\mathrm{R}} = r\alpha\, S \displaystyle\int_0^L \dfrac{F(x)\left[F_{\mathrm{in}} - F(x)\right]}{k + F(x)}\,dx$ $= \alpha v S \left[F_{\mathrm{in}} - F(L)\right]$	$N^{\mathrm{c}}_{\mathrm{R}} = r\alpha V \dfrac{F^{\mathrm{c}}\left(F^{\mathrm{c}}_{\mathrm{in}} - F^{\mathrm{c}}\right)}{k + F^{\mathrm{c}}}$ $= \alpha c V \left(F^{\mathrm{c}}_{\mathrm{in}} - F^{\mathrm{c}}\right)$
Total population	$N_{\mathrm{T}} = \alpha S \displaystyle\int_0^L \left[F_{\mathrm{in}} - F(x)\right]dx$	$N^{\mathrm{c}}_{\mathrm{T}} = \alpha V \left(F^{\mathrm{c}}_{\mathrm{in}} - F^{*}\right)$
Active population	$N_{\mathrm{A}} = \alpha S \displaystyle\int_0^{x^{*}} \left[F_{\mathrm{in}} - F(x)\right]dx, \quad x^{*}: F(x^{*}) = k$	$N^{\mathrm{c}}_{\mathrm{A}} = N^{\mathrm{c}}_{\mathrm{T}}$
Fixation probability	$\mathcal{F} = \dfrac{\int_0^L R(x_{\mathrm{M}})\frac{M(x_{\mathrm{M}})}{B(x_{\mathrm{M}})}dx_{\mathrm{M}}}{\int_0^L R(x_{\mathrm{M}})dx_{\mathrm{M}}}$	$\mathcal{F}^{\mathrm{c}} = \dfrac{N_{\mathrm{M}}}{N^{\mathrm{c}}_{\mathrm{T}}}$
Washout limit	$v_{\mathrm{wo}} = \begin{cases} \dfrac{rL}{k/F_{\mathrm{in}}+1} \\[2ex] \sqrt{\dfrac{4rD}{k/F_{\mathrm{in}}+1}} \end{cases}$	$c = \dfrac{r}{k/F^{\mathrm{c}}_{\mathrm{in}} + 1}$

Table S2: Comparison of the main derived quantities in the spatial system and the chemostat.

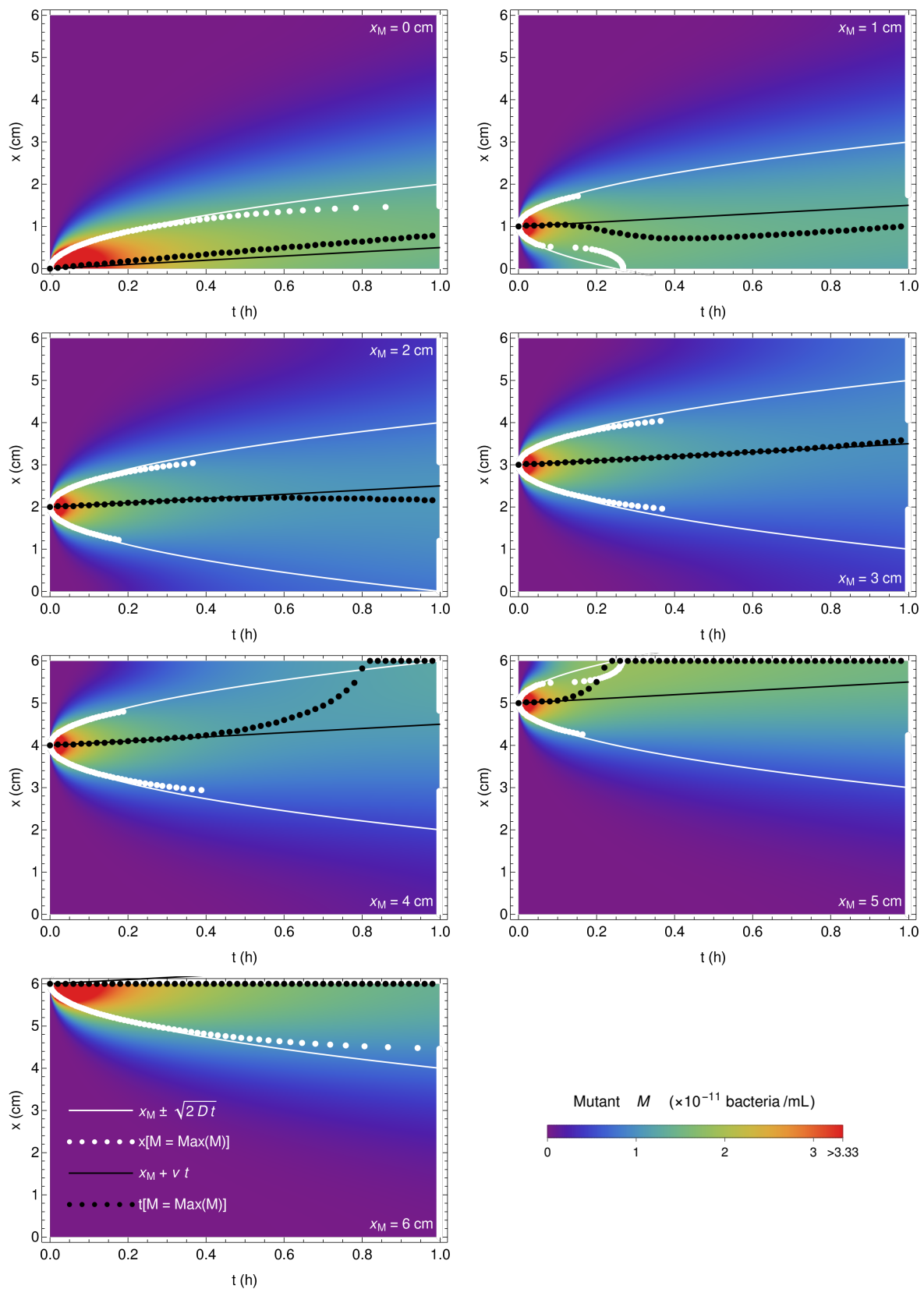# S5   Early dynamics of mutant bacteria concentration

Figure S4: Early dynamics of mutant concentration. Spatio-temporal evolution of mutant concentration for $x_M = 0, 1, 2, 3, 4, 5, 6$ cm in the first hour after mutant introduction. Black points correspond to the maximum mutant concentration at time t, white points correspond to the maximum mutant concentration at position x, black line is $x_M + vt$, and white curve is $x_M \pm \sqrt{2Dt}$. The parameter values are $D = 0.4 \, \text{cm}^2/\text{h}$, $v = 0.5 \, \text{cm/h}$, $k = 0.1 \, \text{mM}$, $r = 0.42 \, \text{h}^{-1}$, $v \, F_{\text{in}} = 1 \, \text{mM cm/h}$, $\alpha = 6.13 \times 10^8$ bacteria/(mL mM) and $M_0 = 3.33 \times 10^{-9}$ bacteria/mL.

S6 Stationary state of mutant bacteria concentration versus the initial position x_{M} of mutants
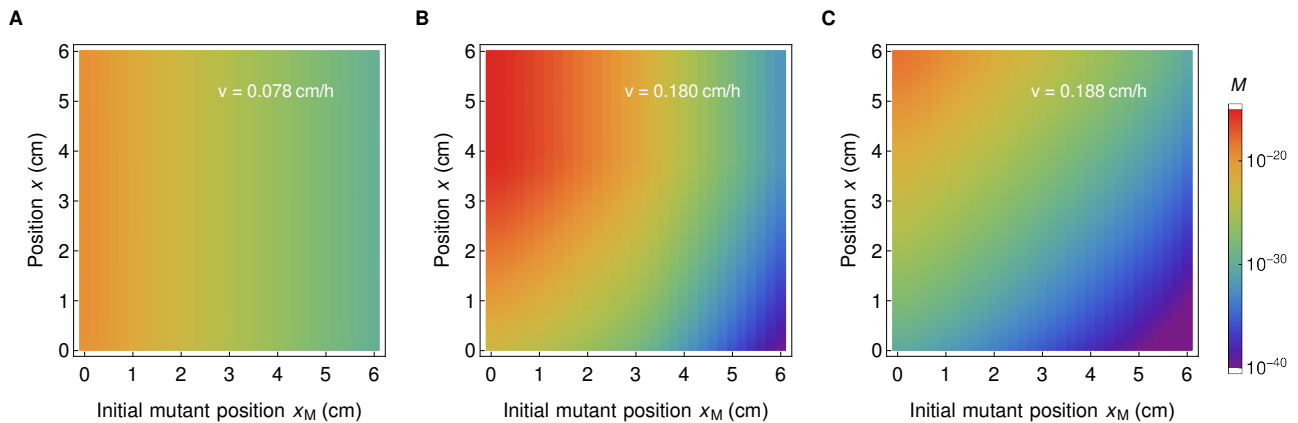

Figure S5: Stationary distribution of mutant bacteria in the gut. Concentration of mutant bacteria as a function of position x, and initial mutant position x_{M}, for $D = 0.02\,\mathrm{cm}^2/\mathrm{h}$, and for three different values of flow velocity v, corresponding to the flat concentration profile in the well mixed regime (**A**), spatial concentration profile (**B**), and close to the washout limit (**C**). In all three cases, we observe that the final concentration of the mutant bacteria is smaller if the initial position x_{M} is further along the gut. This figure corresponds to three points of the top curve in Fig. 3.
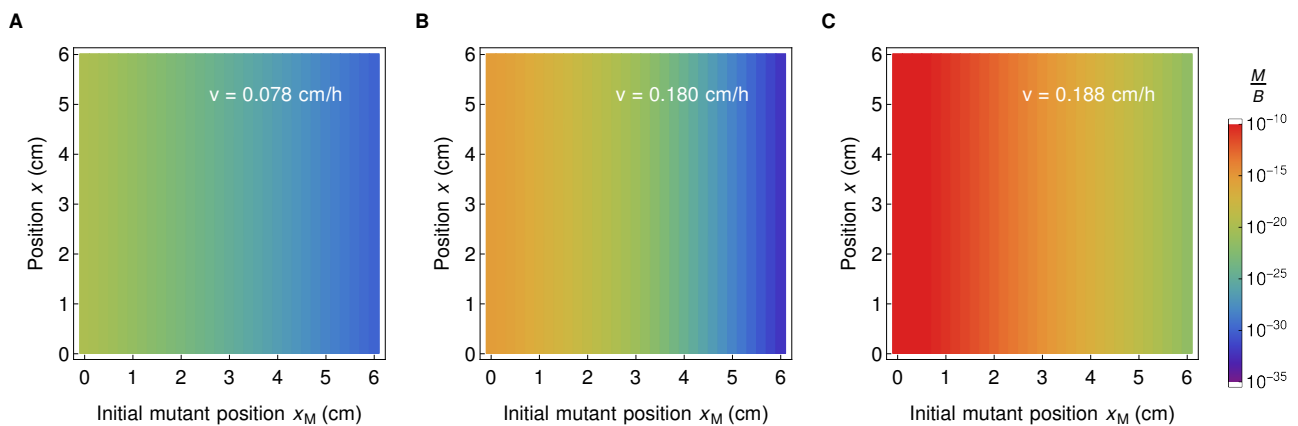

Figure S6: Stationary ratio of mutant to wild type bacteria concentrations. The ratio M/B is shown in all three cases corresponding to Fig. S5. Consistently with our analytical predictions discussed in the main text, the M/B ratio is constant along the gut. In addition, we observe that it monotonically decreases as a function of initial mutant position x_{M}, and the decrease is the most pronounced in the case of the spatial profile (panel **B**) where the ratio at the beginning and at the end of the gut are several orders of magnitude apart.

S7 Location where most mutants that fix originate

While the position of the maximum of the ratio M/B of mutant to wild type bacteria concentrations is always at the entrance of the gut (see main text and Figure 2), the position of the maximum of the number R of reproduction events per unit volume and unit time depends on parameter values. We find that for flat concentration profiles, it is located either close to the entrance of the gut (for small velocities yielding an almost well-mixed system) or at the exit of the gut (close to the washout limit). Conversely, for spatial concentration profiles, its location is intermediate (see Figure S7A). Because of this, in the regime with strong spatial dependence, we find that the position of the maximum of the product $R\,M/B$ of these two quantities ranges between 0 and $L/2$ (see Figure S7B and C). The position of the latter maximum corresponds to the location where most mutants that fix tend to originate.
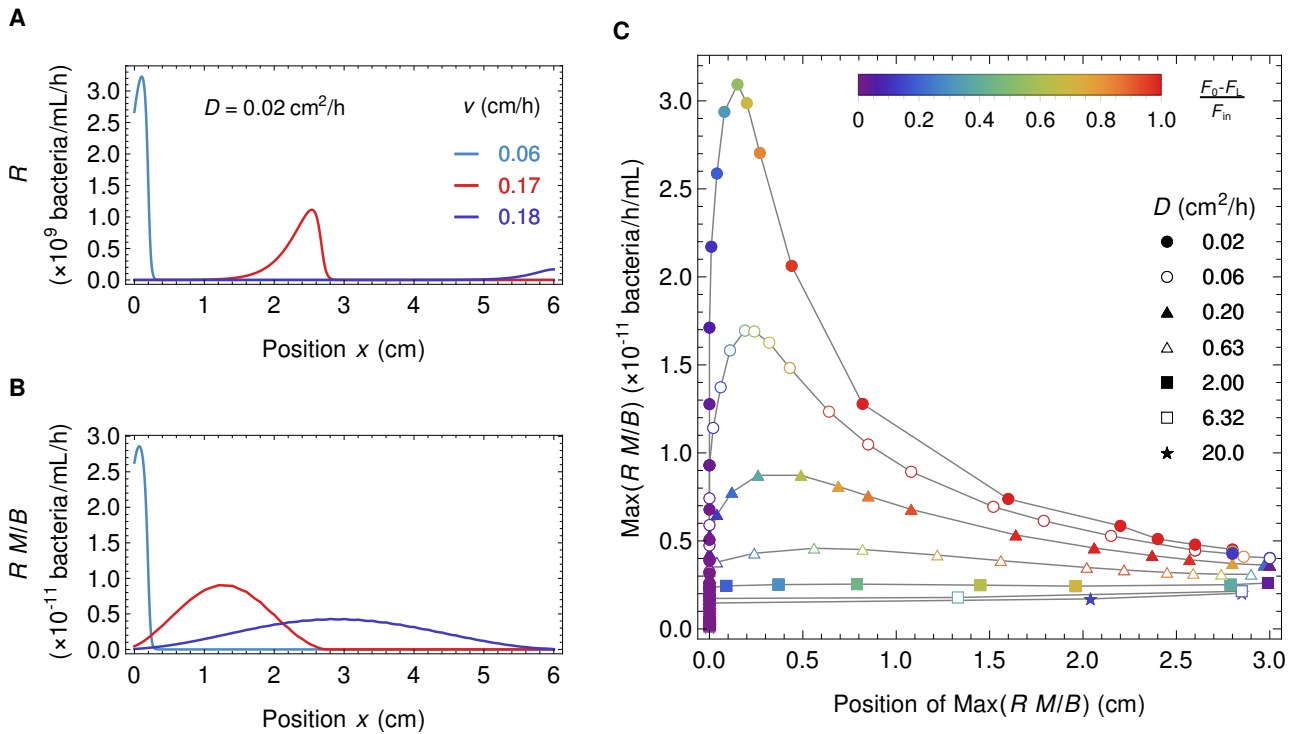

Figure S7: Maximum of R and $R\,M/B$. A: Number R of reproduction events per unit volume and unit time as a function of position along the gut for three different types of concentration profiles, almost well-mixed (light blue), spatial (red), and close to the washout limit (purple). **B:** Maximum of the product $R\,M/B$ of the reproduction events per unit volume and unit time and of the ratio of mutant and wild type bacteria as a function of space for the same three concentration profiles as in A (same colors). **C:** Maximum value of $R\,M/B$ as a function of its position for the data set in Figure 3 of the main text.

S8 Calculation of the active population size

The active population corresponds to the bacteria in the zone where reproduction rate is significant. Concretely, it is defined as

$$N_{\mathrm{A}} = S \int_0^{x^*} B(x)dx \,, \tag{44}$$

where x^* corresponds to the point in the gut segment where the food concentration equals the Monod constant k, i.e. $F(x^*) = k$, implying that the reproduction rate $\rho(x^*)$ is equal to half of the maximal possible reproduction rate, which is obtained if $F(x) \gg k$. Thus,

$$B(x^*) = \alpha[F_{\mathrm{in}} - F(x^*)] = \alpha[F_{\mathrm{in}} - k] = \alpha F_{\mathrm{in}}(1 - \kappa) \,. \tag{45}$$

In the active population thus defined, the reproduction rate of bacteria is at least equal to half of its maximal possible value.

S9   Impact of the dimensionless parameters

S9.1   Holding the dimensionless parameters fixed

To illustrate the relevance of the dimensionless parameters introduced in section S2.2 to describe the stationary profiles, we vary system parameters so that we hold the dimensionless ones fixed. The reference for fixing them is Figure 2:

$$\kappa = \frac{k}{F_{\text{in}}} = \frac{0.1}{2.0} = 0.050, \tag{46}$$

$$\lambda = \frac{rD}{v^2} = \frac{0.42 \times 0.2}{0.5^2} = 0.34, \tag{47}$$

$$\sigma = \frac{Lv}{D} = \frac{6 \times 0.5}{0.2} = 15. \tag{48}$$

We first vary the gut length L in order to ease the discretization of the space. Once the L is chosen, the dimensionless parameters are fixed by adjusting v, and then F_{in}, to keep the product $v\,F_{\text{in}}$ constant. Other parameters are kept fixed. Figure S8A shows the corresponding concentration profiles. They all have the same shape, as evidenced by rescaling the food concentration by F_{in} and the spatial coordinate by L (see inset of the Figure S8A). Figure S8B shows that the fixation probability for these profiles scales with active population, $\mathcal{F} = N_{\text{M}}/N_{\text{A}}$, consistently with our expectations, since the concentration profiles are strongly spatially dependent.
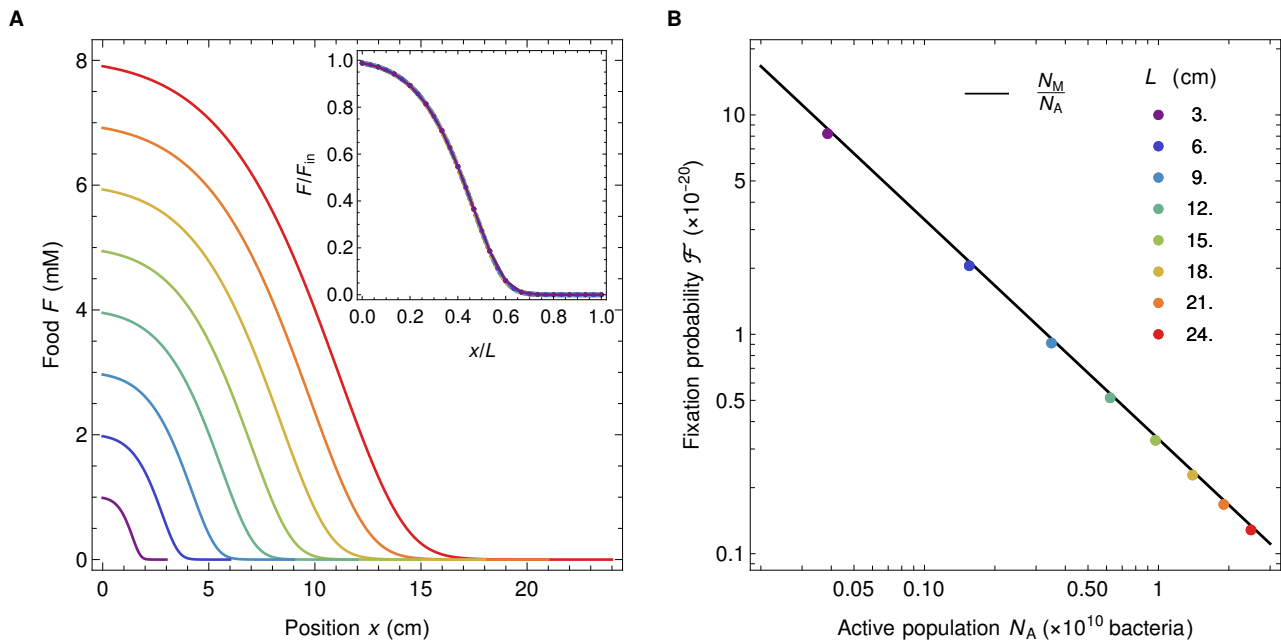

Figure S8:   A Food concentration profiles for different system sizes and keeping nondimensional parameters, λ, κ, σ, fixed. The profiles can be rescaled by dividing food concentration by F_{in} and space by L (see inset of A) showing all the profiles are identical up to the scaling factors. **B** Fixation probability for the profiles in panel **A**. The parameters are $D = 0.2\,\text{cm}^2/\text{h}$, $v = 3./L$ cm/h, $F_{\text{in}} = 1./v$ mM, $k = 0.05/v$ mM, $r = 1.68 \cdot v^2$ h^{-1}, $\alpha = 6.13 \times 10^8$ bacteria/(mL mM), $N_{\text{M}} = 3.33 \times 10^{-11}$ bacteria and the L values are listed in the panel **B**.

S9.2   Range of the dimensionless parameters

In this section, we discuss the range of values of the dimensionless parameters κ, λ and σ, which are the only parameters of the model that may change the behavior of the system and affect our conclusions (recall that α is just a scaling factor that does not affect spatial profiles and conclusions, see section S1.3). We first discuss the range of values that these dimensionless parameters take in our study and in Refs. [39, 40], and then we address the realistic range of values that they can take in the human gut, and compare them together.

The parameter values employed in this paper correspond to the mini gut described in [39], where it has been proven that the mathematical model describes well the experimental setup. In [40], the same model was used to describe microbiota growth and composition in the human colon, and parameter values were thus altered to match the properties of the human gut, which is several times bigger than the mini gut. However, this change of parameter values did not significantly modify the values of the dimensionless parameters. As illustrated in

Figure S8, holding the dimensionless parameters fixed fully preserves the properties of the system, including the spatial profiles of concentrations, and our conclusions on the active population remain true. Table S3 summarizes the range of dimensionless parameter values considered in Figure 3 of this paper, and compares them to those of Refs. [39, 40].

Dimensionless parameter	Figure 3	Figure 3; $\frac{F(0)-F(L)}{F_{\text{in}}} > 0.9$	Ref. [39]	Ref. [40]
$\kappa = \dfrac{k}{F_{\text{in}}}$	$10^{-4} - 0.21$	$0.014 - 0.083$	0.05	2.5×10^{-4}
$\lambda = \dfrac{rD}{v^2}$	$0.19 - 8.4 \times 10^6$	$0.24 - 0.42$	$0.036 - 9.3$	0.29
$\sigma = \dfrac{Lv}{D}$	$3 \times 10^{-4} - 57$	$7.59 - 56$	$1.5 - 25$	9.6

Table S3: Dimensionless parameter values used in Figure 3 of this paper and in Refs. [39] and [40].

Let us now discuss the realistic range of values of the dimensionless parameters κ, λ and σ in the human gut. Let us start by considering $\kappa = k/F_{\text{in}}$, and for this, let us first estimate F_{in}. Bacteria in the large intestine consume a mix of different nutrients that have not (or not completely) been absorbed in the small intestine. A large component of them are fibers, and a human typically ingests 25 to 100 g a day of fibers [4]. The colon input also includes a smaller or similar quantity of unabsorbed sugars and starch [61]. Given that the inflow of digesta in the colon is about 2 liters per day [62], the order of magnitude of the incoming food concentration F_{in} in the colon is in the range of 15 to 100 g/L. The Monod constant k depends on many factors, including the substrate and the bacterial strain. Even for glucose, it can range from 0.03 to 5 mg/L depending on how well adapted the bacteria are to growing on glucose [63], and it is typically higher for other substrates (20 to 300 mg/L for acetate [64]; 5 to 900 mg/L for different substrates [65]). Realistic values for $\kappa = k/F_{\text{in}}$ are thus in a wide range, but in all cases, they are much smaller than 1, at least as small as 0.1. In the next section where dimensionless parameter values are systematically varied, Figure S9 demonstrates that such values of κ give very similar outcomes, and all results collapse in the limit $\kappa \to 0$.

The two other dimensionless parameters, λ and σ, both involve the effective diffusion coefficient D, which models mixing and is thus hard to measure directly. However, it is empirically well demonstrated that there is a strong gradient of bacterial concentration along the colon [66, 67], and that most nutrients that could be used by bacteria are consumed by the end of the gut [61]. This requires that $\lambda = rD/v^2$ be larger than $1/4$ (washout limit, see section S3), and less than a few units (since above, diffusion is strong enough for the system to be almost well mixed). This can be seen on Figure 1C. Accordingly, Table S3 demonstrates that despite the wide range of parameters used in our study, the range of λ is very narrow in the regime that yields strongly spatial profiles (specifically, λ is between 0.24 and 0.42 when $[F(0) - F(L)]/F_{\text{in}} > 0.9$). This is in line with the estimate from [40].

Let us finally turn to σ. We notice that $\sigma = Lv/D = Lr/(v\lambda)$. Avoiding washout requires $L/v > (\kappa+1)/r \gtrsim 1/r$ (see section S3), where the last inequality is rather tight because $\kappa \ll 1$. Since in addition $1/\lambda$ is of the order of 2 to 4 in the very spatial regime, $\sigma = Lr/(v\lambda)$ then has to be greater than a few units. Another way to estimate σ is to employ $Lr/v = \tau_{\text{dig}}/\tau_{\text{rep}}$ where $\tau_{\text{rep}} = 1/r$ is the typical replication time, and $\tau_{\text{dig}} = L/v$ is the typical time spent in the system. While the total transit time ranges from one to several days [68], the time spent by the digesta in the ascending colon, which is the upstream part of the colon where the strong gradients of food and bacterial concentrations are located [40], is substantially shorter, of the order of 4 hours [69], and thus $\tau_{\text{dig}} \approx 4$ h. Let us now estimate τ_{rep}. Feces weigh about 130 g/day and contain 25–50% of bacteria in mass [4]. The typical mass of a bacteria being 1 pg, this means that about 3–6×10^{13} bacteria per day are lost in feces, to be compared with about 4×10^{13} bacteria in the colon [1], leading to about one renewal per day, which means that $\tau_{\text{rep}} \leq 24$ h. However, as it is likely that bacteria actively replicate only in the upper part of the colon, while r represents the maximal reproduction rate in the gut, the actual value of τ_{rep} is expected to be substantially smaller than this upper bond. A lower bound for τ_{rep} is given by the minimal doubling time of fast replicating bacteria such as *Escherichia coli* in good conditions, which can be as low as 20 minutes [70]. To summarize, $\sigma = \tau_{\text{dig}}/(\lambda\tau_{\text{rep}})$, with $1/\lambda$ of the order of 2–4 and $\tau_{\text{dig}}/\tau_{\text{rep}} \gtrsim 1$, and $\tau_{\text{dig}}/\tau_{\text{rep}} \approx 10$ when considering the ascending colon and the maximal replication rate. This matches well the range of values of σ considered in the present work (see Table S3).

S9.3 Varying each dimensionless parameter

Finally, we systematically investigate the impact of each dimensionless parameter by varying one of them while holding the other two fixed. We keep parameters v, D and F_{in} fixed throughout, and vary k, r, and L one at a time in order to change κ, λ, and σ, respectively. Results in Figures S10, S9 and S11 show that the fixation probability is well described by $\mathcal{F} = N_{\text{M}}/N_{\text{A}}$ except in cases where the food concentration profile is less spatial because food is substantially depleted even at the entrance of the gut, which occurs for the four largest values of r in Figure S10.
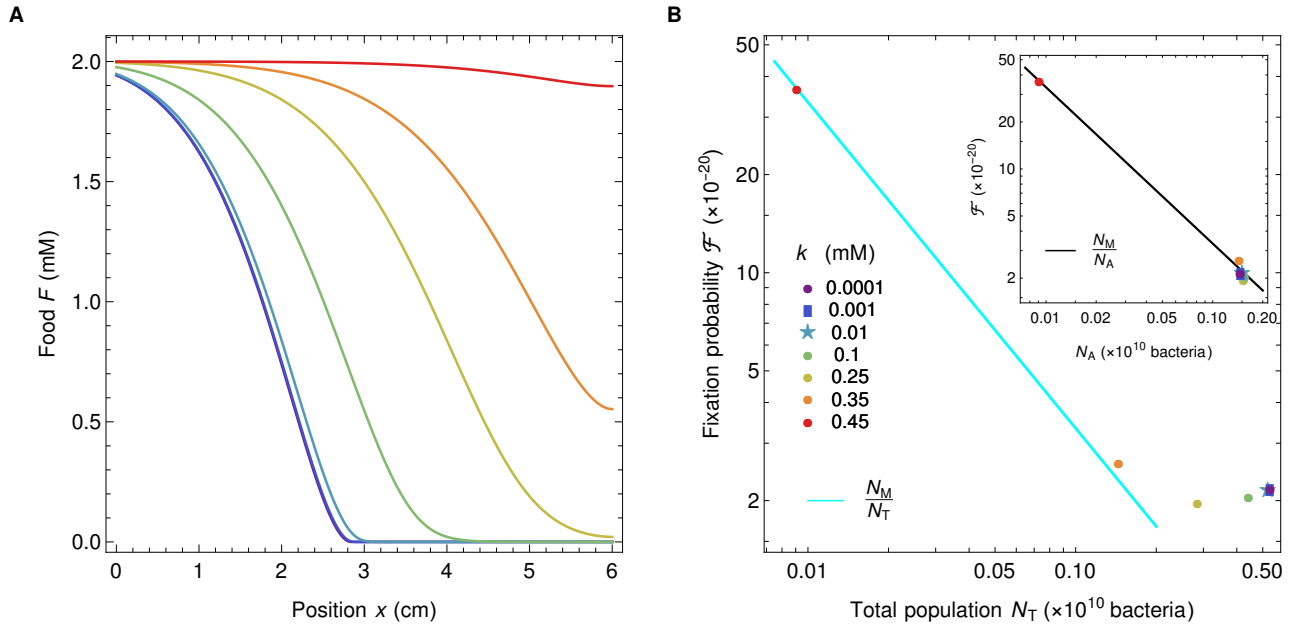

Figure S9: Varying κ. **A** Food profiles for different values of κ and fixed $\lambda = 0.336$ and $\sigma = 15$. **B** Fixation probability as a function of total population N_{T} and active population N_{A} (in the inset). Different colors correspond to different values of κ (k) and different symbols are used for overlapping data points. Parameters are $v = 0.5\,\text{cm/h}$, $D = 0.2\,\text{cm}^2/\text{h}$, $L = 6.0\,\text{cm}$, $r = 0.42\,\text{h}^{-1}$, $\alpha = 6.13 \times 10^8\,\text{bacteria}/(\text{mL}\,\text{mM})$, and $N_{\text{M}} = 3.33 \times 10^{-11}\,\text{bacteria}$. k values are listed in the panel **B**.
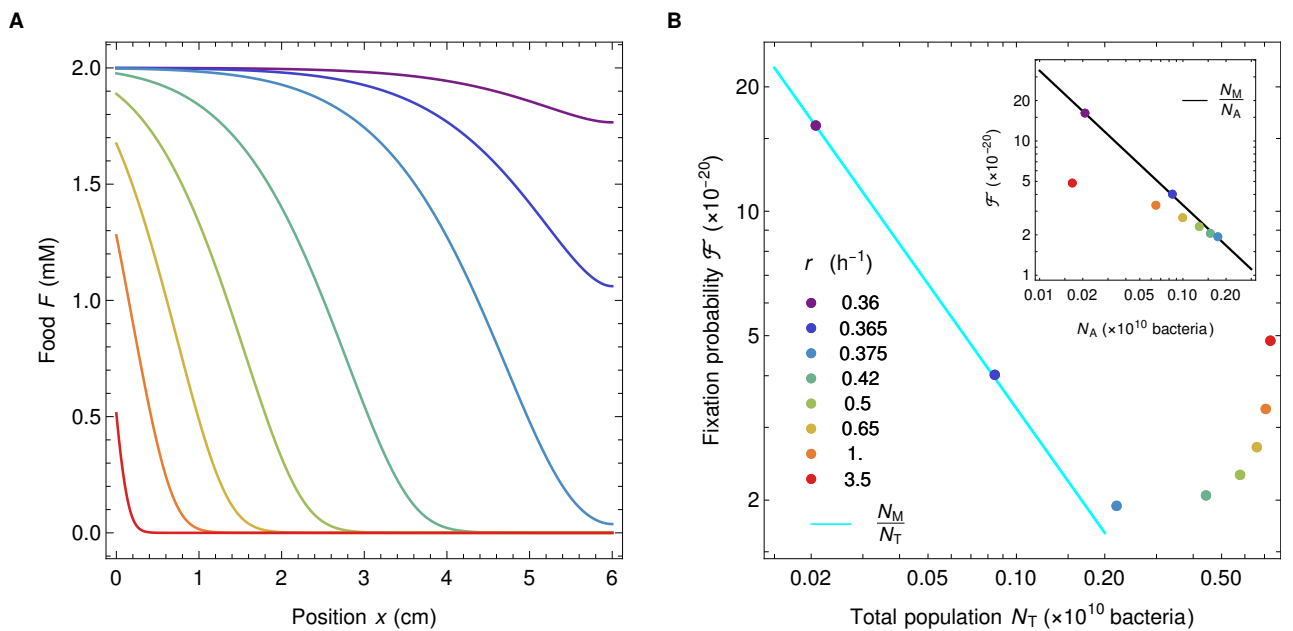

Figure S10: Varying λ. **A** Food profiles for different values of λ and fixed $\kappa = 0.05$ and $\sigma = 15$. **B** Fixation probability as a function of total population N_{T} and active population N_{A} (in the inset). Different colors correspond to different vales of λ (r). Parameters are $v = 0.5\,\text{cm/h}$, $D = 0.2\,\text{cm}^2/\text{h}$, $k = 0.1\,\text{mM}$, $k = 0.1\,\text{mM}$, $\alpha = 6.13 \times 10^8\,\text{bacteria}/(\text{mL}\,\text{mM})$, and $N_{\text{M}} = 3.33 \times 10^{-11}\,\text{bacteria}$. r values are listed in the panel **B**.
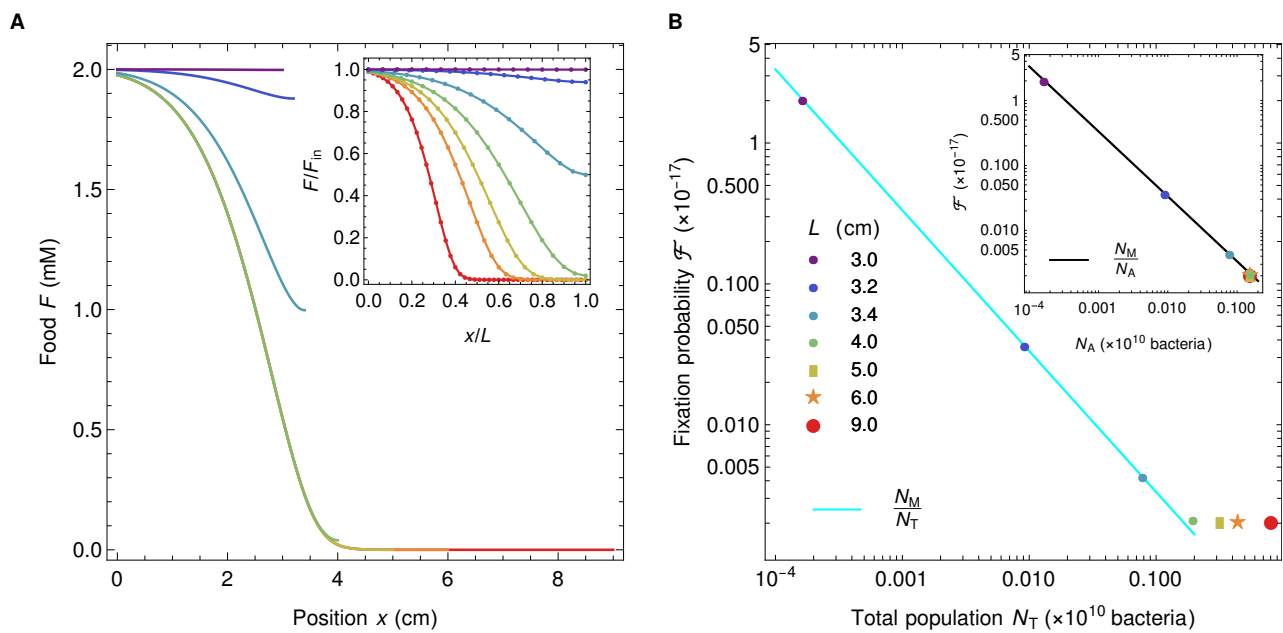
A

B

Figure S11: Varying σ. A Food profiles for different values of σ and fixed $\lambda = 0.336$ and $\kappa = 0.05$. The inset shows rescaled food profiles, for easier comparison of the spatial dependence. **B** Fixation probability as a function of total population N_{T} and active population N_{A} (in the inset). Different colors correspond to different values of σ (L) and different symbols are used for overlapping data points. Parameters are $v = 0.5\,\mathrm{cm/h}$, $D = 0.2\,\mathrm{cm}^2/\mathrm{h}$, $L = 6.0\,\mathrm{cm}$, $r = 0.42\,\mathrm{h}^{-1}$, $\alpha = 6.13 \times 10^8\,\mathrm{bacteria/(mL\,mM)}$, and $N_{\mathrm{M}} = 3.33 \times 10^{-11}\,\mathrm{bacteria}$. k values are listed in the panel **B**.